Geophys. J. Int. (2009) **177,** 691–716 doi: 10.1111/j.1365-246X.2008.04059.x

Glacial rebound and plate spreading: results from the first countrywide GPS observations in Iceland

T. Árnadóttir,[1] B. Lund,[2] W. Jiang,[1]* H. Geirsson,[3] H. Björnsson,[4] P. Einarsson[4] and T. Sigurdsson[5]

[1]*Nordic Volcanological Center, Institute of Earth Sciences, University of Iceland,* IS-101 *Reykjavík, Iceland. E-mail: thora1@hi.is*
[2]*Department of Earth Sciences, Uppsala University, Villavägen* 16, 752 36 *Uppsala, Sweden*
[3]*Physics Department, Icelandic Meteorological Office, Reykjavík, Iceland*
[4]*Institute of Earth Sciences, University of Iceland,* IS-101 *Reykjavík, Iceland*
[5]*National Land Survey of Iceland, Akranes, Iceland*

Accepted 2008 December 10. Received 2008 December 5; in original form 2008 June 12

SUMMARY

Iceland is one of the few places on Earth where a divergent plate boundary can be observed on land. Direct observations of crustal deformation for the whole country are available for the first time from nationwide Global Positioning System (GPS) campaigns in 1993 and 2004. The plate spreading across the island is imaged by the horizontal velocity field and high uplift rates ($\geq$10 mm yr^{-1}) are observed over a large part of central and southeastern Iceland. Several earthquakes, volcanic intrusions and eruptions occurred during the time spanned by the measurements, causing local disturbances of the deformation field. After correcting for the largest earthquakes during the observation period, we calculate the strain rate field and find that the main feature of the field is the extension across the rift zones, subparallel to the direction of plate motion. Kinematic models of the horizontal plate spreading signal indicate a slightly elevated rate of spreading in the Northern Volcanic Zone (NVZ) (23 $\pm$ 2 mm yr^{-1}), while the rates at the other plate boundary segments agree fairly well with the predicted rate of plate spreading ($\sim$20 mm yr^{-1}) across Iceland. The horizontal ISNET velocities across north Iceland therefore indicate that the excessive spreading rate (>30 mm yr^{-1}) observed by GPS in 1987–1992 following the 1975–1984 Krafla rifting episode was significantly slower during 1993–2004. We model the vertical velocities using glacial isostatic adjustment (GIA) due to the recent thinning of the largest glaciers in Iceland. A layered earth model with a 10-km thick elastic layer, underlain by a 30-km thick viscoelastic layer with viscosity 1 $\times$ 10^{20} Pa s, over a half-space with viscosity $\sim$1 $\times$ 10^{19} Pa s can explain the broad area of uplift in central and southeastern Iceland. A wide area of significant residual uplift (up to 8 mm yr^{-1}) is evident in north Iceland after we subtract the rebound signal from the observed rates, whereas the Reykjanes Peninsula and the Western Volcanic Zone (WVZ) appear to be subsiding at a rate of 4–8 mm yr^{-1}. We observe a coherent pattern of small but significant residual horizontal motion (up to 3 mm yr^{-1}) away from Vatnajökull and the smaller glaciers that is most likely caused by glacial rebound. Our study demonstrates that the velocity field over a large part of Iceland is affected by deglaciation and that this effect needs to be considered when interpreting deformation data to monitor subglacial volcanoes in Iceland.

Key words: Satellite geodesy; Plate motions; Glaciology; Kinematics of crustal and mantle deformation; Rheology: crust and lithosphere.

1 INTRODUCTION

Geodetic measurements, in particular Global Positioning System (GPS) observations, have for the most part confirmed the basic concept of plate tectonics that the Earth's surface can be divided into a number of rigid plates. Thus, plate motion models derived

*Now at: GPS Research Center, Wuhan University 129 Luoyu Road, Wuhan 430079, China.

from geodetic data spanning less than three decades agree remarkably well with the models based on observations spanning millions of years (e.g. DeMets *et al.* 1990, 1994; Sella *et al.* 2002). The other main assumption of the theory of plate tectonics is that the plate boundaries are narrow regions where the relative plate motion is accommodated. This assumption is proving to be less well founded, as many plate boundaries are diffuse with the deformation accommodated over a wide area. Strain rates of stable plate interiors are bounded between 1 and 10×10^{-12} yr^{-1}, with strain rates in diffuse plate boundaries as high as $\sim 10^{-8}$ yr^{-1} (Gordon 1998). Therefore, in order to test the theory of plate tectonics in a particular region, one needs very accurate observations of crustal deformation to determine which areas can be classified as rigid plates and to estimate the width of plate boundary zones.

Since the initiation of the theory of plate tectonics, Iceland has been recognized as one of the few places on the Earth where direct observations of extensional processes related to plate spreading are possible. This is due to its location on the Mid-Atlantic ridge, straddling the boundary between the North American and Eurasian plates. The plate boundary in Iceland is, however, more complex than at a typical mid-ocean ridge due to the interaction between the ridge and the Iceland hotspot, resulting in extensive volcanism, anomalously thick crust, low viscosity, as well as repeated ridge jumps generating overlapping rift zones, transforms and oblique spreading.

In this paper, we present the horizontal and vertical velocity fields for the whole of Iceland, derived from GPS campaign measurements in 1993 and 2004, termed ISNET (Valsson *et al.* 2007). The ISNET velocities depict the broad features of the deformation in Iceland, imaged by the 20- to 30-km station spacing. The measurements span 11 yr, resulting in a large signal-to-noise ratio for the velocities, which is particularly important for determining the vertical component of the signal. As a result, we are able to resolve a significant rate of vertical uplift in central Iceland, with a maximum of the same order of magnitude as the rate of spreading ($\sim$20 mm yr^{-1}). Such a coherent view of the uplift has not been obtained previously. We apply finite element (FE) models of glacial isostatic adjustment (GIA) due to volume changes of the four largest glaciers in Iceland to explain the broad vertical uplift signal we observe. The horizontal velocities show spreading across the active volcanic zones, confirming results obtained from prior, more localized studies of plate boundary deformation in Iceland. We construct a kinematic model describing the plate boundary deformation in Iceland, assuming that the boundary can be approximated by a series of rectangular dislocations. We estimate the locking depth on the dislocations as well as the rates of opening and/or strike-slip motion. Our preferred model also includes several Mogi point sources, representing active volcanic centres.

1.1 Geodetic studies of plate boundary deformation in Iceland

The plate boundary in Iceland is composed of overlapping volcanic rift zones and transform zones. Plate spreading is mainly accommodated by extension across the volcanic zones and horizontal shear in the transform areas (Fig. 1). In the southwest, the Reykjanes segment of the Mid-Atlantic Ridge comes onshore at the Reykjanes Peninsula. The oblique plate motion on the Reykjanes Peninsula appears to be mostly accommodated by left-lateral shear along a zone striking N80°E (Hreinsdóttir *et al.* 2001), though a significant component of opening has been suggested by recent studies (Árnadóttir *et al.* 2006; Keiding *et al.* 2008). Volcanic fissure swarms trend NE, whereas faulting occurs on N–S right-lateral strike-slip faults, which are nearly perpendicular to the trend of the plate boundary. At the Hengill triple junction, the rift branches into the Western Volcanic Zone (WVZ) and the South Iceland Seismic Zone (SISZ). The SISZ is a transform zone, where the relative E–W plate motion appears to be accommodated by shear below $\sim$15 km depth (Árnadóttir *et al.* 2006) and by moderate size earthquakes (M6–7) rupturing parallel N–S right-lateral strike-slip faults in the brittle crust in a manner described as 'book-shelf' faulting (Einarsson *et al.* 1981; Sigmundsson *et al.* 1995). In 2000 June, an earthquake sequence occurred in the SISZ, when two $M_w = 6.5$ earthquakes ruptured two parallel N–S striking faults within a span of 3 days (Stefánsson *et al.* 2003). This sequence continued with a $M_w = 6.3$ earthquake in the western part of the SISZ on 2008 May 29.

At the eastern edge of the SISZ, the plate boundary continues northeastwards along the Eastern Volcanic Zone (EVZ). Hence, there are two overlapping rift zones in south Iceland, the WVZ and the EVZ. The Thingvellir graben is the prominent tectonic feature in the WVZ. The infrequent post-glacial eruptions and the large topographic relief indicate that the WVZ is a magma starved rift (Sæmundsson 1992). The EVZ is comprised of several NE trending overlapping volcanic fissure swarms. The most significant rifting episode of recent centuries in the EVZ was the 1783–1784 Laki eruption. This eruption produced the largest volume of erupted material in historic time in Iceland (Thordarson & Larsen 2007). One of Iceland's most active volcanoes, Hekla, is located near the intersection of the SISZ and the EVZ. Southwards from this intersection lies an area of alkaline volcanism, the Eastern Volcanic Flank Zone (EVFZ) with geochemical and structural characteristics of a propagating rift (Jóhannesson *et al.* 1990). Several active volcanoes are in the EVFZ, including the subglacial volcanoes Katla, beneath Mýrdalsjökull, and the Eyjafjallajökull volcano.

GPS studies in south Iceland indicate that most of the spreading is presently occurring across the EVZ with a smaller component of extension across the WVZ (Sigmundsson *et al.* 1995; LaFemina *et al.* 2005). From GPS observations spanning 1994–2003, LaFemina *et al.* (2005) concluded that the amount of extension across the WVZ and the EVZ varies along the strike of each rift zone from north to south. Constructing two profiles spanning both the WVZ and the EVZ, they found that 2-D models of opening in an elastic half-space could match the data, assuming almost the full spreading rate (19.0 ± 2.0 mm yr^{-1}) below the northern part of the EVZ decreasing to about 11.0 ± 0.8 mm yr^{-1} in southern EVZ. Conversely, they estimated a rate of opening of about 2.6 ± 0.9 mm yr^{-1} in the northern part of the WVZ, increasing to 7.0 ± 0.4 mm yr^{-1} across the Thingvellir graben. This lateral variation in the spreading rates is in agreement with simple models of ridge propagation, supporting the notion that the WVZ is becoming extinct, while the EVZ is propagating southwestwards (Einarsson 1991). The sum of the extension rates in the direction of plate motion (N102°E) across the two rift zones is approximately 18–20 mm yr^{-1}, in agreement with predictions from the REVEL model of plate motion (Sella *et al.* 2002). As a result of the overlapping spreading segments in south Iceland, the existence of a microplate, termed the Hreppar block, has been suggested in the area between the WVZ and the EVZ (Einarsson 1991; Sigmundsson *et al.* 1995; LaFemina *et al.* 2005).

The Mid-Iceland Belt (MIB) is a volcanic zone in central Iceland, connecting the northern parts of the WVZ and the Northern Volcanic Zone (NVZ) (Thordarson & Larsen 2007). Several central volcanoes are located beneath Vatnajökull glacier near the inferred centre of the Icelandic hotspot (e.g. Wolfe *et al.* 1997). The most

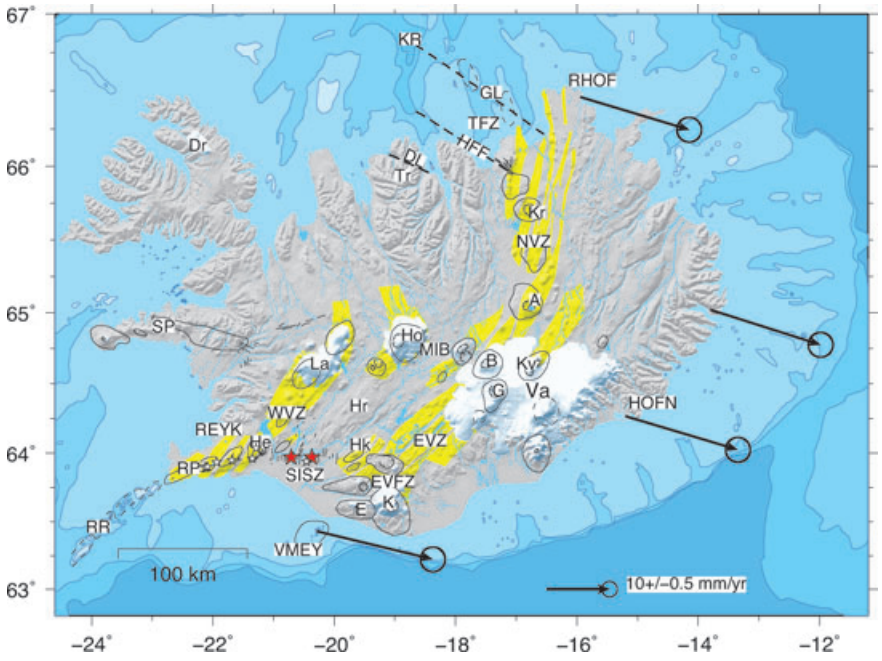

Figure 1. A map indicating the active plate boundary in and around Iceland: the Reykjanes Ridge (RR), the Reykjanes Peninsula (RP), the Western Volcanic Zone (WVZ), the South Iceland Seismic Zone (SISZ), the Eastern Volcanic Flank Zone (EVFZ), the Eastern Volcanic Zone (EVZ), the Mid-Iceland Belt (MIB), the Northern Volcanic Zone (NVZ), the Tjörnes Fracture Zone (TFZ) [i.e. the Dalvík Lineament (DL), the Húsavík–Flatey Fault (HFF), the Grímsey Lineament (GL), shown with dashed lines] and the Kolbeinsey Ridge (KR). The yellow areas show individual fissure swarms with associated central volcanoes (black ellipses). The largest glaciers are in order of decreasing area: Vatnajökull (Va), Langjökull (La), Hofsjökull (Ho), Mýrdalsjökull (K), Drangajökull (Dr) and Eyjafjallajökull (E). The most recently active volcanoes in Iceland are Hengill (He), Hekla (Hk), Katla (K), Grímsvötn (G), Bárdarbunga (B), Kverkfjöll (Kv), Askja (A) and Krafla (Kr). The location of the Hreppar block is indicated (Hr), Snæfellsnes Peninsula (SP) and Tröllaskagi Peninsula (Tr). Mapped surface faults of Holocene earthquakes in the SISZ are shown with thin black lines lines (Einarsson & Sæmundsson 1987). The epicentre locations of $M_w \geq 5$ earthquakes in 1998, 2000 June and 2003 August are shown with white stars, and the 2000 June main shocks ($M_w = 6.5$) with red stars. The location of Reykjavík, the capital of Iceland, is labelled by REYK. The black arrows show the spreading directions and magnitudes (full rate in mm yr^{-1}) of CGPS stations (VMEY, HOFN and RHOF) located on the Eurasian plate relative to stable North America predicted by the NUVEL-1A plate motion model (DeMets *et al.* 1994).

currently active of these are the Grímsvötn and Bárdarbunga volcanoes. North of Vatnajökull, the plate boundary continues as the NVZ. The NVZ consists of five volcanic systems comprised of fissure swarms and central volcanoes, such as Kverkfjöll, Askja and Krafla. At least three rifting episodes have occurred in the NVZ in historical time, two in the Krafla volcanic system (1724–1729 and 1975–1984) and one in the Askja volcanic system during 1874–1875. The most recent, and hence best documented, rifting episode in Iceland took place in the Krafla volcanic system from 1975 December to 1984 September (e.g. Björnsson 1985; Einarsson 1991). During the 9-yr period, over 20 intrusive events and nine eruptions were observed along approximately 80 km of the fissure swarm, causing up to 9 m of extension (Tryggvason 1994). The average widening during the Krafla rifting episode was about 5 m, corresponding to about 250 yr of plate spreading. GPS measurements in north Iceland spanning 1987–1990 indicated significantly increased rates of extension (up to 56 mm yr^{-1}) across the NVZ (Foulger *et al.* 1992; Jahn 1992), compared to the steady-state rate of 19–20 mm yr^{-1} predicted by plate motion models. The velocity increase observed in the first GPS campaigns in north Iceland (1987–1992) has been attributed to post-rifting transient deformation following the 1975–1984 Krafla rifting event (e.g. Foulger *et al.* 1992; Heki *et al.* 1993; Hofton & Foulger 1996). Subsequent GPS observations in north Iceland in 1992–1995 indicate decaying rates, approaching the long-term average (e.g. Völksen 2000).

At the north coast, the plate boundary continues northwestwards offshore along the Tjörnes Fracture Zone (TFZ), a complex zone of right-lateral transform motion and extension, that connects the NVZ and the Kolbeinsey Ridge. Seismicity in the TFZ occurs mostly along three lineaments trending NW–SE: the Grímsey lineament (GL), the Húsavík–Flatey fault (HFF) and the less active Dalvík lineament (Einarsson 1991; Rögnvaldsson *et al.* 1998). The HFF is a mature, WNW trending right-lateral strike-slip fault. Earthquakes on the GL occur on northerly oriented faults, with the seismicity following an overall NW trend. The GL is currently more seismically active than the HFF. Similar to the SISZ, the largest earthquakes in the TFZ reach $M \sim 7$. The most recent moderate size earthquake on the TFZ was a $M_S = 6.4$ event in 1976 on the GL (NEIC). The TFZ is a complex region and the mostly offshore locations of the main transforms hamper geodetic studies of the deformation in the area and their interpretation. The continuous GPS (CGPS) network in Iceland is rapidly expanding as a result of international collaboration (Geirsson *et al.* 2007). The new CGPS network includes 10 stations installed in north Iceland in 2006, with the aim of significantly improving our understanding of the area.

1.2 Glacial isostatic adjustment studies

There have been several studies on GIA in Iceland in recent years, based on data such as lake levels (Sigmundsson & Einarsson 1992),

GPS vertical uplift rates (e.g. Thoma & Wolf 2001; Sjöberg *et al.* 2004; Fleming *et al.* 2007; Pagli *et al.* 2007a), gravity (Jacoby *et al.* 2001; Hartmann *et al.* 2007) and seismic receiver functions (Kumar *et al.* 2005). These studies have focused on the retreat of the Vatnajökull ice cap and the ensuing rebound, and relevant data have, therefore, generally been collected in the vicinity of the glacier. The rheological structure beneath Vatnajökull is inferred using 2-D or axisymmetric model approximations of the glacier geometry. The earth models employed in these studies have varied considerably, from very simple elastic plate on viscoelastic half-space models (e.g. Pagli *et al.* 2007a) to more elaborate multilayered models with a low-viscosity asthenosphere (e.g. Fleming *et al.* 2007), a lithosphere low-viscosity channel (Kumar *et al.* 2005) and a mantle plume (Hartmann *et al.* 2007). Although the varying earth structures used in these studies make direct comparison of the results a little difficult, the viscosity beneath Vatnajökull is inferred to be low, with estimates ranging from 1×10^{17} Pa s (Sjöberg *et al.* 2004) via $1–2 \times 10^{18}$ Pa s (Fleming *et al.* 2007) and $4–10 \times 10^{18}$ Pa s (Pagli *et al.* 2007a) to 5×10^{19} Pa s (Sigmundsson & Einarsson 1992). The estimated thickness of the elastic layer, frequently referred to as the lithosphere, varies between approximately 10 and 30 km in these studies. In light of the viscosities inferred beneath Vatnajökull, the disappearance of the large ice sheet of the latest Ice Age (about 10 000 yr BP) no longer produces a rebound signal detectable above the noise levels in current GPS data.

Most of the above studies utilize the ice loss estimate for Vatnajökull reported by Sigmundsson & Einarsson (1992): 182 km^3 between 1890 and 1973. However, Pagli *et al.* (2007a) recently presented a revised ice volume loss estimate for Vatnajökull of 435 km^3 between 1890 and 2003. This increase in the melting rate estimate has a profound effect on the inferred rheological structure of the region, which may explain the difference in the viscosities estimated by Pagli *et al.* (2007a) and Fleming *et al.* (2007).

Turning from Vatnajökull, Pinel *et al.* (2007) studied both annual and long-time load variations in the Mýrdalsjökull glacier, using GPS data and a Green's function method which allows a 2-D distribution of surface load sources. Based on arguments of the ratio of vertical to horizontal deformation, they infer that the deformation observed around Mýrdalsjökull cannot be due solely to glacial rebound. Instead, Pinel *et al.* (2007) argue that the magma inflow into a shallow magma chamber in the Katla volcano between 1999 and 2004 is required to explain the observations. In a study which considers seasonal melting at multiple glaciers, Grapenthin *et al.* (2006) use the same Green's function approach in order to model annual fluctuations in time series from CGPS stations in Iceland. They conclude that the seasonal signals can be explained by annual variations in the ice load at the four largest glaciers in Iceland, and infer a minimum value of the Young's modulus for an elastic half-space of 40 ± 15 GPa.

1.3 Earthquakes and volcano deformation during 1993–2004

Several $M_w \geq 5$ earthquakes and magmatic events occurred during the time period spanned by the ISNET measurements (see Fig. 2). The largest earthquakes were two $M_w = 6.5$ events that ruptured 10–15 km long N–S faults in the SISZ in 2000 June (Stefánsson *et al.* 2003; Clifton & Einarsson 2005; Hjaltadóttir *et al.* 2005; Antonioli *et al.* 2006). Before calculating the ISNET station velocities and the strain rates, we correct the time series at stations affected by coseismic displacements due to the 2000 June earthquake sequence using models obtained in previous studies (Pedersen *et al.* 2003; Árnadóttir *et al.* 2004). We correct the ISNET velocity field for the coseismic offsets due to these earthquakes, but several stations in the SISZ are also affected by post-seismic deformation following the events (Árnadóttir *et al.* 2005).

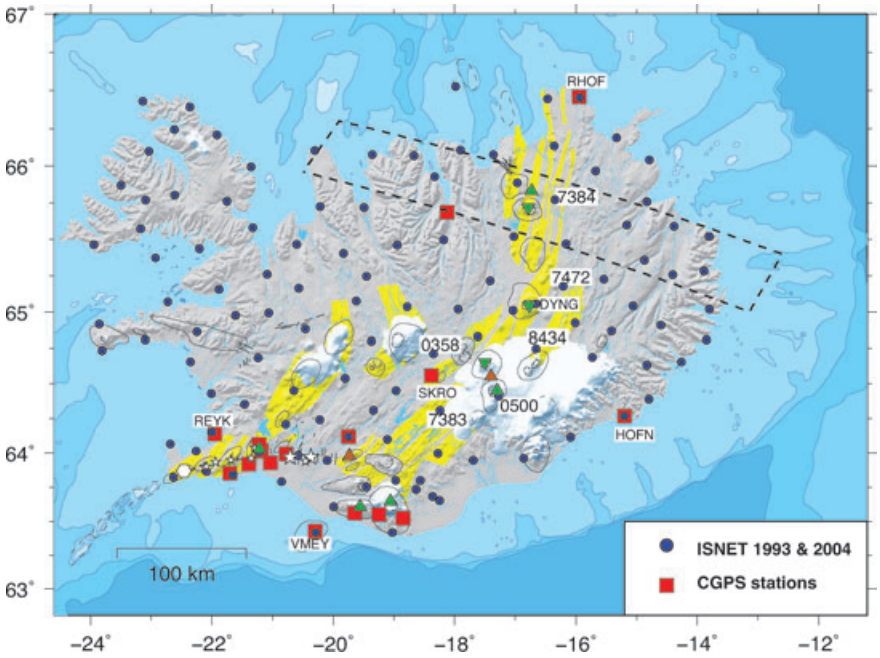

Figure 2. Locations of the ISNET campaign GPS stations (blue circles) and continuous GPS stations (red squares). Stations discussed in the text are labelled. Central volcanoes are shown with black ellipses and fissure swarms are shown in yellow. The epicentres of $M_w \geq 5$ earthquakes are shown with white stars. Triangles denote volcanic centres of magmatic activity during the 1993–2004 time intervals. Green triangles indicate uplift or intrusions, inverted green triangles subsidence and orange triangles denote eruptive sites. The white hexagon shows the location of the Svartsengi geothermal field. The black box drawn with a dashed line outlines the stations included in the horizontal velocity profile shown in Fig. 12.

In addition to earthquakes, the data include deformation associated with magmatic activity. The most significant of these events are, in order of longitude from west to east, increased seismic activity and uplift at the Hengill triple junction between 1994 and 1998 (Sigmundsson *et al.* 1997; Feigl *et al.* 2000; Vogfjörd *et al.* 2005), the 2000 February eruption of Hekla volcano (Ágústsson *et al.* 2000; Höskuldsson *et al.* 2007), the 1994 and 1999 intrusions into Eyjafjallajökull (Pedersen & Sigmundsson 2004, 2006), increased seismicity and uplift at the Katla subglacial volcano since 1999 (e.g. Sturkell *et al.* 2008), the 1996 October Gjálp eruption (Gudmundsson *et al.* 2004; Pagli *et al.* 2007b), the 1998 December Grímsvötn eruption (Sturkell *et al.* 2003) and deflation of Askja volcano since 1983 (Pagli *et al.* 2006; Sturkell *et al.* 2006). The Krafla caldera has been subsiding at a variable rate since 1989 (Sturkell *et al.* 2006). A broad uplift signal was detected in an area north of Krafla using synthetic aperture radar interferometry (InSAR) spanning 1993–1999 (de Zeeuw-van Dalfsen *et al.* 2004), which has been interpreted as indication of magma accumulation at ∼20 km depth in the Krafla system, rather than post-rifting adjustments.

2 GPS OBSERVATIONS AND DATA ANALYSIS

A nationwide GPS campaign network in Iceland (ISNET) was first surveyed in 1993 August, when a total of 119 stations were measured for at least one 8-hr session each. Four stations were measured throughout the campaign (Supporting Information, Table S1). The station coordinates of the 1993 survey were used to generate a geodetic datum for Iceland (ISN93). During 2004 August 2, a total of 115 of the GPS stations observed in 1993 were resurveyed (Fig. 2). Most of the stations were occupied for two 12- to 16-hr sessions. The latter survey was used to update the geodetic datum for Iceland (ISN2004) (Valsson *et al.* 2007). The first continuous GPS (CGPS) station in Iceland has been running since 1995 in Reykjavík (REYK) and the second station in Höfn (HOFN) since 1997. Both these stations belong to the International GNSS Service (IGS) network and are operated by the Bundesamt für Kartographie und Geodäsie (BKG) in Germany and the National Land Survey of Iceland. An Icelandic network of continuous GPS stations (ISGPS) has been operated since early 1999 by the Icelandic Meteorological Office (IMO) (Geirsson *et al.* 2006).

We analysed the GPS data from both ISNET surveys, including data from 16 CGPS stations in Iceland, to estimate the crustal deformation field for the whole of Iceland. The data analysis was carried out with the GAMIT/GLOBK software (Herring *et al.* 1990; Herring 2003; King & Bock 2003), using standard procedures (McClusky *et al.* 2000). We first estimate parameters such as station position and orbital trajectory on a daily basis for a given 24-hr interval from combining three data sets: (1) the campaign stations, (2) the continuously operating GPS stations in Iceland (including the two IGS stations REYK and HOFN) and (3) long-running CGPS stations within 5000 km of Iceland (ALGO, MADR, ONSA, TROM and WES2). The details of the data processing are as described by, for example, McClusky *et al.* (2000). The initial orbits are based on the precise satellite orbital parameters determined by the Scripps Institute of Oceanography (SIO) (Bock *et al.* 1997) for the 1993 ISNET survey and the IGS solutions (Beutler *et al.* 1994) for the 2004 ISNET and CGPS observations. After the daily parameter estimation, we combine the loosely constrained solutions with three global IGS subnetworks (IGS1, IGS3 and EURA), using the GLOBK software (Herring 2003) in a regional stabilization approach (McClusky *et al.* 2000). To define a consistent reference frame for all epochs, we combine all daily solutions using Helmert-like transformations to estimate translation, rotation, scale and earth orientation parameters (polar motion and UT1 rotation). This stabilization procedure defines a reference frame by minimizing, in the least-square sense, the departure from *a priori* values based on the International Terrestrial Reference Frame 2005 (ITRF2005) (Altamimi *et al.* 2007), of the positions and velocities for a set of 22 well-determined stations in and around Iceland. Thus, we obtain the coordinates and velocities of the stations in a reference frame that is approximately aligned with the ITRF2005. To decrease the sensitivity of the frame to any errors in the vertical velocities we assign lower weight (larger prior uncertainty) to the vertical velocity estimates by a factor of 10. We then estimate the positions and velocities of the other stations with respect to the frame defined by the stabilization. For the continuously observing stations, we place a lower bound on their uncertainties by adding 2 and 5 mm of white noise to the horizontal and vertical components, respectively, to account for the correlation between successive estimates for the station positions. A few of the ISNET stations are affected by the 2000 June earthquake sequence. Before calculating the station velocities and the strain rates, we therefore correct the time series of these stations for coseismic offsets using predicted station displacements from the models of Pedersen *et al.* (2003) and Árnadóttir *et al.* (2004). The resulting horizontal and vertical station velocities in the ITRF2005 are given in Table S1 (Supporting Information). Our velocity estimates are about 0.1–0.2, 0.6–0.7 and 0.7–1.0 mm yr^{-1} higher, in east, north and vertical, respectively, in the ITRF2005 than if we use the ITRF2000 frame. This is a smaller difference in the vertical rates than the 1.6 mm yr^{-1} suggested by Altamimi *et al.* (2007).

3 THE 1993–2004 GPS VELOCITY FIELD

3.1 Horizontal velocities

We estimate the surface velocities for the whole of Iceland in the ITRF2005, and then determine the horizontal velocities relative to stable North America to accentuate the plate boundary deformation. The transformation was done with GLOBK using the absolute rotation pole for North America in the ITRF2005 (Altamimi *et al.* 2007). The resulting station velocities, relative to stable North America, are shown in Fig. 3 and Table S2 (Supporting Information).

In this reference frame, stations on the North American plate have small velocities compared to stations on the Eurasian plate. Fig. 3 shows that the horizontal velocities are small in western and northwestern Iceland, confirming that those stations are located on the stable North American plate. The east component of the velocity increases dramatically as we move eastwards across the plate boundary and onto the Eurasian plate. The velocities of stations farther than 50–100 km from the plate boundary are consistent with the predicted velocities from the NUVEL-1A plate motion model (DeMets *et al.* 1994) (green arrows in Fig. 3). The CGPS station RHOF, which is east of the Grímsey seismic lineament has a velocity that is slightly slower than the predicted NUVEL-1A velocity, as does the CGPS station VMEY in south Iceland. The horizontal velocity at the IGS station HOFN (in SE Iceland) appears to be a little faster than the NUVEL-1A prediction. These velocity deviations are, however, only 1–3 mm yr^{-1}, and therefore marginally significant, considering the uncertainties of the observations and of the NUVEL-1A model predictions.

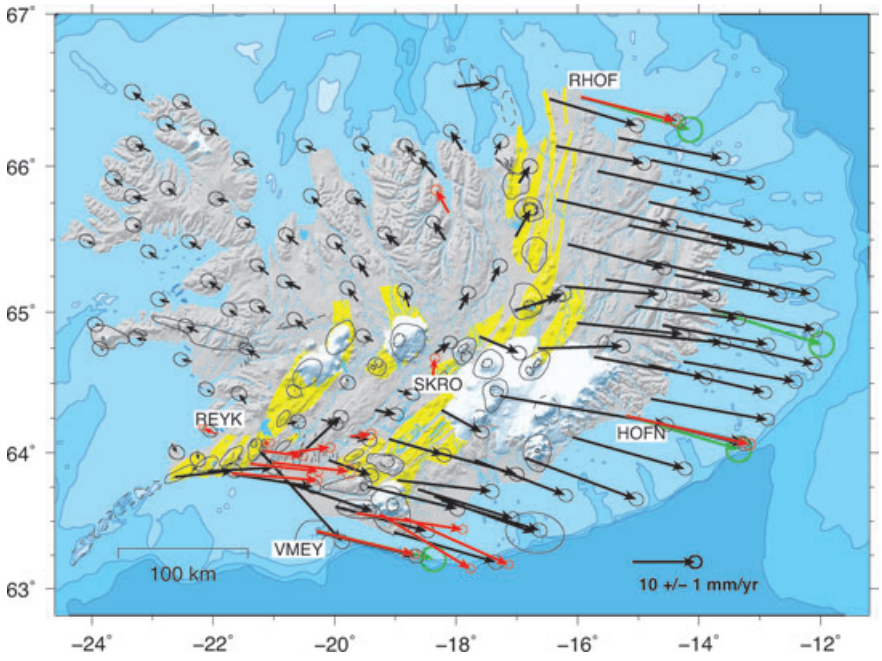

Figure 3. Horizontal GPS station velocities with 95 per cent confidence ellipses, relative to stable North America, determined from the ISNET measurements spanning the time interval 1993–2004 (black arrows) and CGPS stations in Iceland for the time interval 1999–2004 (red arrows). The predicted velocity of Eurasia relative to stable North America from the NUVEL-1A plate motion model (DeMets *et al.* 1994) is shown with green arrows.

In southern Iceland, a significant increase in horizontal velocities is evident across the Reykjanes Peninsula, the SISZ and the EVZ. This confirms conclusions from prior studies, indicating that the plate motion is primarily accommodated across these parts of the plate boundary in southern Iceland (e.g. Sigmundsson *et al.* 1995; Hreinsdóttir *et al.* 2001; LaFemina *et al.* 2005; Árnadóttir *et al.* 2006). The stations near the western edge of the active rift zone move towards the zone, relative to the North American plate, because these stations are located within the plate boundary zone, and hence do not move at the full plate rate. A gradual increase in the eastward component of the velocity is apparent across southern central Iceland, in the proposed Hreppar block, i.e. the area between the two overlapping rift zones (the WVZ and the EVZ). We do not estimate the Euler vector for the Hreppar block as there are only five ISNET stations located on the block, and their velocities are potentially affected by post-seismic deformation following the 2000 June earthquake sequence. Further studies are needed to determine whether the area of the proposed Hreppar block is truly a rigid microplate and, if so, the nature of the MIB, that forms the northern boundary of that plate, or whether the area is a sliver of crust that is presently caught between the two overlapping rift zones in south Iceland, and will eventually become part of the North American plate as the WVZ becomes extinct.

To examine possible local deformation in the eastern part of Iceland, we estimate the horizontal ISNET velocities relative to stable Eurasia by transforming the station velocities using the absolute rotation pole for the motion of Eurasia in the ITRF2005 determined by Altamimi *et al.* (2007). In this reference frame stations moving with the Eurasian plate should have small velocities. Fig. 4, however, shows that several stations have significant residual velocity relative to the Eurasian plate. In particular, an interesting, nearly radial pattern of horizontal motion decreasing away from Vatnajökull is evident in the eastern part of Iceland. This pattern indicates deformation that is not predicted by plate motion models, and hence, most likely due to processes other than plate spreading. Other indications of local deformation processes are observed near active volcanoes. The southward motions of the CGPS stations south of Mýrdalsjökull have been taken as a sign of magma accumulation in Katla (e.g. Sturkell *et al.* 2008). The ISNET station located between the two CGPS stations south of Katla, however, does not show a similar trend. This velocity difference between the ISNET and CGPS stations could be attributed to surface deformation caused by proposed magma accumulation at shallow depth at Katla in the time interval spanned by the CGPS observations (1999–2004), as the CGPS stations are located closer to the volcano than the ISNET stations, and their time series cover the short time interval suggested for the Katla inflation (Pinel *et al.* 2007; Sturkell *et al.* 2008). The large eastward velocity at station 0500 (at Grímsvötn) is most likely caused by magma accumulation at shallow depth below the volcano, as the ISNET measurements span the 1998 eruption and inflation periods before and after the eruption (Sturkell *et al.* 2003). A small eastward component of motion is also observed at station 7384 located NE of Krafla, which may be an indication of deep magma accumulation (de Zeeuw-van Dalfsen *et al.* 2004), or post-rifting deformation.

3.2 Vertical velocities

We estimate the average vertical velocities for the 1993–2004 time interval, in the ITRF2005 reference frame as described above. Fig. 5 shows a broad zone of uplift in central Iceland, with a maximum of about 23 mm yr^{-1} at the CGPS station SKRO. The vertical rates decay towards southwest and northwest, while they remain high along the southeast coast. The broad pattern of uplift in central and southeast Iceland as well as the subsidence on the Reykjanes Peninsula have been noted in previous GPS studies (e.g. Hreinsdóttir *et al.* 2001; Sjöberg *et al.* 2004; Árnadóttir *et al.* 2006; Geirsson *et al.* 2006; Pagli *et al.* 2007a), although those observations cover a smaller area than the ISNET network. The uplift around Vatnajökull

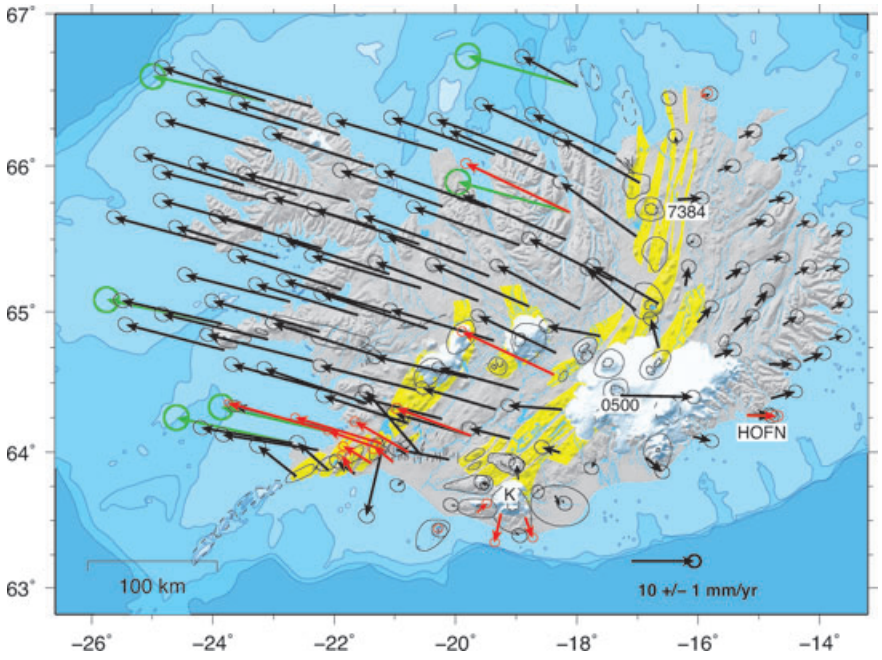

Figure 4. Horizontal GPS station velocities with 95 per cent confidence ellipses, relative to stable Eurasia, estimated from the ISNET observations for the time interval 1993–2004 (black arrows) and CGPS stations in Iceland for the time interval 1999–2004 (red arrows). The predicted velocity of North America relative to stable Eurasia from the NUVEL-1A plate motion model (DeMets *et al.* 1994) is shown with green arrows.

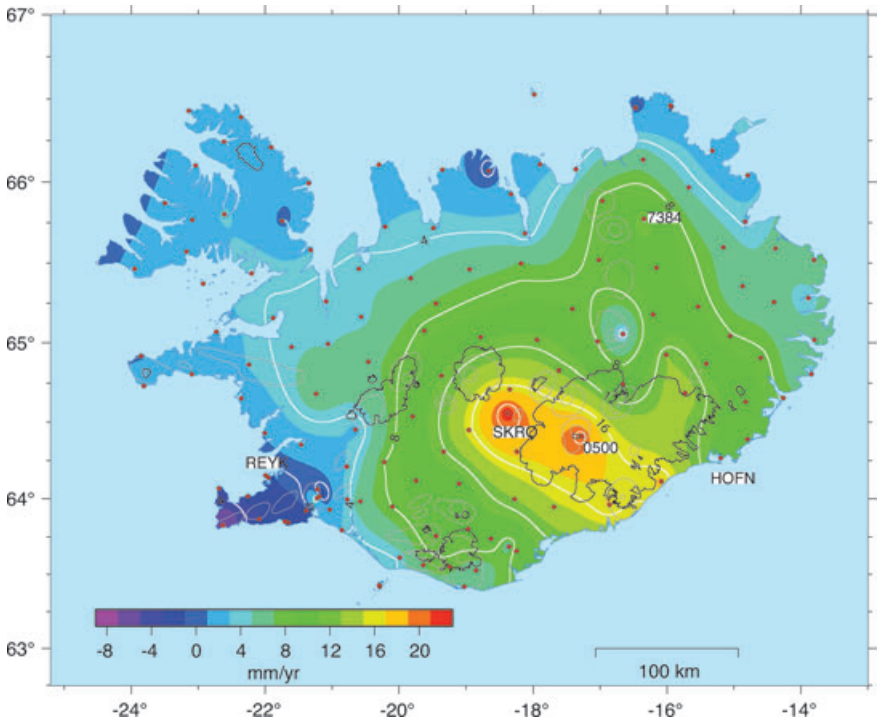

Figure 5. Vertical velocities in the ITRF2005 from ISNET (1993–2004) and the CGPS network in Iceland (1999–2004). Positive numbers indicate uplift and negative are subsidence. Contour lines are drawn every 4 mm yr^{-1}. The red dots show the GPS station locations.

has been explained by models of glacial rebound due to the thinning of Vatnajökull (e.g. Thoma & Wolf 2001; Sjöberg *et al.* 2004; Fleming *et al.* 2007; Pagli *et al.* 2007a). The extensive area of uplift in central Iceland indicates that the rebound due to the melting of the smaller ice caps also needs to be considered when interpreting the ISNET measurements.

A zone of uplift extends northwards, from east central Iceland along the NVZ. This pattern of uplift in the NVZ is perturbed by local subsidence around Askja volcano, appearing as less rapid uplift in Fig. 5. This is in general agreement with previous geodetic studies, indicating that the vertical deformation in the NVZ is concentrated in the areas around Krafla and Askja. Levelling, GPS and

InSAR observations show that the Askja caldera has been subsiding since 1983, possibly even since 1973 (e.g. Pagli *et al.* 2006; Sturkell *et al.* 2006). The Krafla caldera has been subsiding since 1989 (Sturkell *et al.* 2006), but we do not detect this subsidence in the ISNET velocities as no ISNET stations are located within the caldera. A broad uplift signal was detected in the area of maximum 1975–1984 rifting north of Krafla using InSAR observations spanning 1993–1999 (de Zeeuw-van Dalfsen *et al.* 2004). The authors suggest that the signal, about 8 cm of primarily uplift (in the line-of-sight to the satellite) for the 6-yr time interval, is caused by pressure increase at ∼20 km depth, signifying magma accumulation near the crust–mantle boundary in the Krafla system. de Zeeuw-van Dalfsen *et al.* (2004) concluded that the uplift signal could not be due to post-rifting adjustments following the 1975–1984 Krafla rifting episode. We repeated the post-rifting model calculation of Pollitz & Sacks (1996) and found that their preferred model predicts a maximum uplift rate of about 15 mm yr^{-1}, rather than 2 mm yr^{-1} cited by de Zeeuw-van Dalfsen *et al.* (2004). Subsequently, our estimate has been confirmed (F. Pollitz, personal communication, 2007). Hence, the uplift detected by InSAR and the ISNET measurements in the Krafla area could be influenced by post-rifting deformation. The deformation in the Krafla area will be discussed further in Sections 6.2 and 7.2.

The average vertical ISNET velocity at Grímsvötn volcano (station 0500) shows rapid uplift for the time interval 1993–2004. Detailed studies show that the vertical velocity at Grímsvötn varies with time with uplift prior to the 1998 December eruption, coeruptive subsidence and renewed uplift until the 2004 November eruption. The displacements at station 0500 spanning the 1998 December eruption have been interpreted as inflation and coeruptive deflation of a shallow magma source beneath the caldera (Sturkell *et al.* 2003). The average vertical uplift we estimate at station 0500 is therefore influenced by magmatic activity as well as glacial rebound.

The high rate of uplift at the CGPS station SKRO is rather mysterious as this station is neither located near an active central volcano nor at the edge of a fast retreating ice sheet. We suggest that the discrepancy may be due to the different time span of the continuous GPS and ISNET observations. The station SKRO was installed late in the year 2000, and additional GPS campaign observations show that since then, the ISNET station 0358 has a similar vertical rate as SKRO and station 7383, located at the western margin of Vatnajökull, has an even faster vertical rate. The horizontal velocities at the stations SKRO and 0358 are notably different (Fig. 3), possibly due to temporal variation in the rate of deformation or a local source near SKRO. We therefore exclude the velocities from SKRO in our subsequent analysis as it may not represent the average 1993–2004 uplift rates in the area. The GPS station 8434, near Kverkfjöll, has a significantly lower uplift rate than other stations at the edge of Vatnajökull. This station is located near the outlet glacier Dyngjujökull, which surged during 1998–2000 (Björnsson *et al.* 2003; Adalgeirsdóttir *et al.* 2005). InSAR images from 1997 to 1998, spanning the beginning of the surge indicate subsidence in the immediate area near Dyngjujökull (R. Pedersen, personal communication, 2008). The anomalous vertical rate suggests that this station is affected by local deformation caused by the surge and thus we do not include this station in our modelling.

4 STRAIN RATE

One way to estimate the horizontal surface deformation independent of the reference frame is to calculate strain rates from the GPS velocities. Discerning areas with high rates of deformation from more stable regions is sometimes easier from a strain rate map than a velocity map. Here, we use the method described by Beavan & Haines (2001) to estimate the strain rates from our GPS velocities. The method uses a bicubic spline interpolation to estimate the velocities on a rectangular grid. The strain rates are then determined from the spatial derivatives of the velocities, calculated using a finite difference algorithm of the gridded velocities. Smoothing is applied when calculating the strain rates.

We use the following definitions: the coordinate system has the positive x-axis pointing east and the positive y-axis pointing north; u_x and u_y are the respective x- and y-components of displacement, and $\dot{u}_x$ and $\dot{u}_y$ are the respective velocities. The components of the strain rate tensor are:

$$\dot{\varepsilon}_{xx} = \frac{\mathrm{d}\dot{u}_x}{\mathrm{d}x}, \quad \dot{\varepsilon}_{yy} = \frac{\mathrm{d}\dot{u}_y}{\mathrm{d}y}, \quad \dot{\varepsilon}_{xy} = \frac{1}{2}\left(\frac{\mathrm{d}\dot{u}_y}{\mathrm{d}x} + \frac{\mathrm{d}\dot{u}_x}{\mathrm{d}y}\right). \tag{1}$$

Here, we show the strain rates in terms of two quantities: the areal strain rate, calculated from the principal strain rates:

$$(\dot{\varepsilon}_1 + \dot{\varepsilon}_2) = \frac{1}{2}(\dot{\varepsilon}_{xx} + \dot{\varepsilon}_{yy}) \tag{2}$$

and the maximum shear strain rate:

$$|\dot{\varepsilon}_1 - \dot{\varepsilon}_2| = \sqrt{\frac{1}{2}(\dot{\varepsilon}_{xx} - \dot{\varepsilon}_{yy})^2 + \dot{\varepsilon}_{xy}^2}. \tag{3}$$

In order to calculate the strain field from deformation observations, the displacement field must be continuous, meaning that the displacement field should not contain offsets. As explained previously, our data contain signals from several earthquakes, which we have attempted to correct for. In addition, there are a number of other local deformation sources, which may potentially influence the strain calculation. Therefore, we neither include velocities from a station possibly affected by the 1998 June earthquake (0305) in Hengill nor the station at Grímsvötn volcano (0500). We include data only from the CGPS stations REYK and HOFN, since the time series from the other CGPS stations are significantly shorter than the time interval covered by the ISNET observations. The network is, however, too sparse to accurately locate all sources of deformation, but rather the strain rate field provides a general view of the overall plate boundary deformation. The magnitudes of the strain rates we estimate depend on the network geometry, such that excluding stations will tend to lower the strain rates, but enlarge their areal extent.

The results from our strain calculations are shown as areal and maximum shear strain rates in Fig. 6. Low areal and maximum shear strain rates (shown with grey colour) are evident in northwest and east Iceland. The orientation of the principal strain axes are plotted as lines in Fig. 6, black for extension and red for contraction. The principal axes of extension are roughly perpendicular to the axis of spreading, with less contraction along the NVZ and EVZ. In south Iceland, the obliquity (i.e. the angle between the normal to the trend of the plate boundary and the direction of plate motion) ranges from about 15° in the WVZ to almost 70° on the Reykjanes Peninsula. As a result, a similar amount of extension and contraction is observed along the SISZ and the Reykjanes Peninsula, consistent with a stress state favouring strike-slip faulting.

The areal strain rate field estimated from the GPS velocities is characterized by dilatation (positive areal strain rates) along the spreading zones (Fig. 6a). The highest rate of dilatation is found along a narrow elongated region in the NVZ, with a maximum of about 0.3 μstrain yr^{-1} north of Krafla. The narrow region suggests

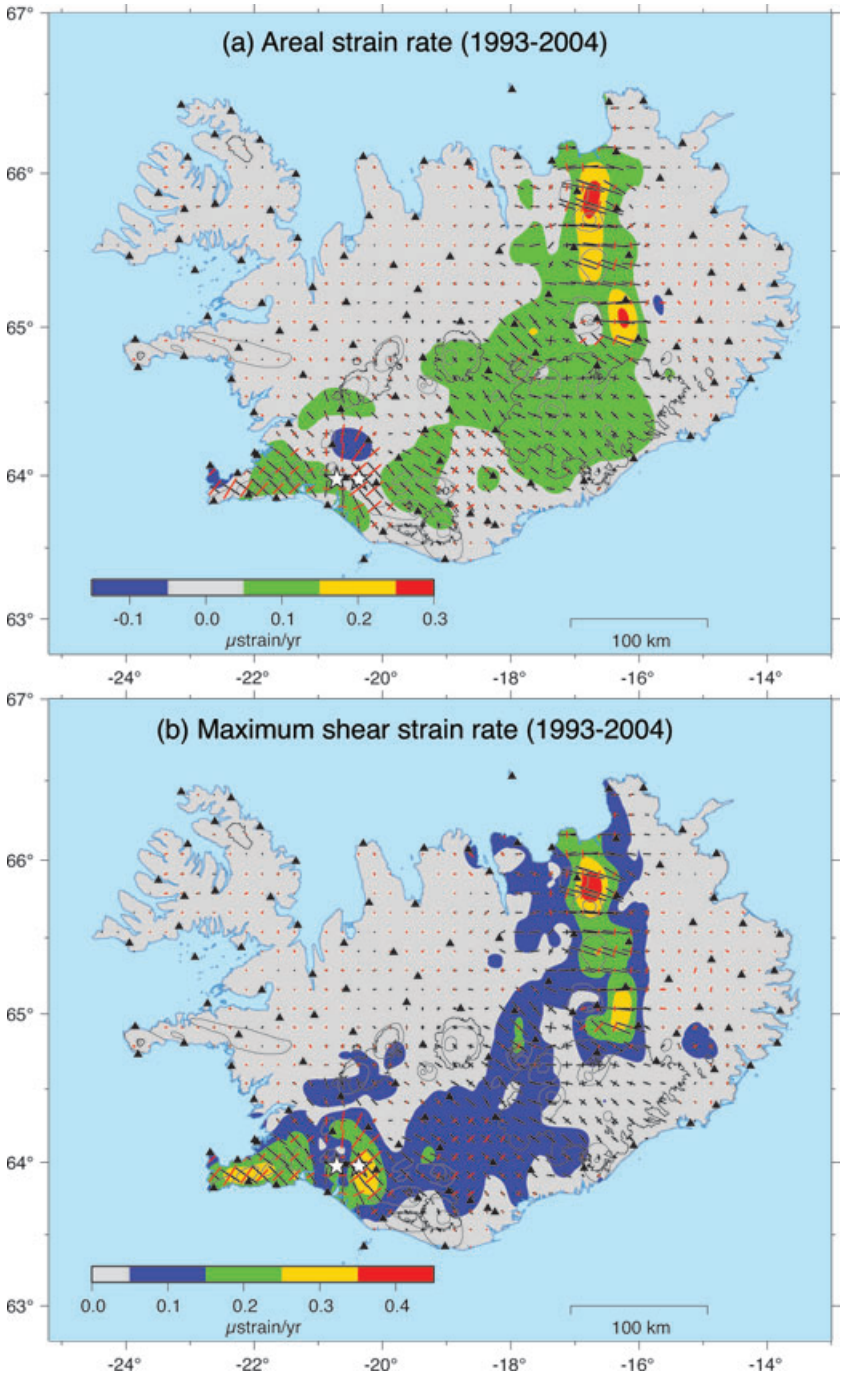

Figure 6. Strain rates calculated from the ISNET station velocities, including data from the CGPS stations HOFN and REYK. The station locations are shown with black triangles and the two $M_w = 6.5$ earthquakes in 2000 June with stars. Outlines of glaciers and central volcanoes are indicated with black and grey lines, respectively. The orientation of the principal strain axes are plotted as lines, black for extension and red for contraction. (a) Areal strain rate ($\dot{\varepsilon}_1 + \dot{\varepsilon}_2$). The warm colours indicate dilatation and the cold colours represent contraction. (b) Maximum shear strain rate ($|\dot{\varepsilon}_1 - \dot{\varepsilon}_2|$).

a shallow source of dilatation in the area. A pattern of relative contraction (or less dilatation) is seen in Askja, as expected due to the ongoing deflation, whereas a zone of high rates of dilatation is evident east of Askja. The GPS station 7472, northeast of Askja, is located at the northern end of a fault that appears to have moved sometime during 1997–1998 (R. Pedersen, personal communication, 2008). The motion during 1997–1998, detected by InSAR analysis is about 1 cm in the line of sight to the satellite (mostly vertical), but the horizontal motion can not be determined from the InSAR data alone. Excluding the GPS station 7472 from the strain calculation still results in a dilatation signal east of Askja suggesting that this signal is not solely due to local deformation near this station. This area has been the source of shallow, persistent earthquake swarm activity since at least the 1980s (Einarsson 1991; Soosalu *et al.* 2008). Faulting appears to be mostly left-lateral strike-slip on NE-striking faults. Furthermore, lower-crustal earthquakes have been detected in this general area since 2006, indicating magmatic movements. An intense swarm of small, lower-crustal earthquakes

has been in progress since early 2007 accompanied by a broad uplift of a few centimetres (e.g. Jakobsdóttir *et al.* 2008). Further south, the zone of extension broadens towards central Iceland. The areas around Hekla and Hengill volcanoes in south Iceland show dilatation, which is most likely related to inflation of magma sources beneath these volcanoes. Contraction caused by subsidence at the geothermal power plant at Svartsengi is evident on the Reykjanes Peninsula (about 0.1 μstrain yr^{-1}), although the signal is shifted NW-wards due to the sparsity of ISNET stations on the peninsula.

The maximum shear strain rate is shown in Fig. 6(b). The predominant E–W left-lateral transform motion due to plate spreading is evident along the Reykjanes Peninsula and the SISZ, with maximum shear strain rates of about 0.3 μstrain yr^{-1}. The maximum shear strain rate in the SISZ is also affected by post-seismic deformation in the epicentral area of the main shocks. The 2000 June main shocks ruptured two right-lateral N–S oriented faults in the SISZ. Post-seismic deformation due to viscoelastic flow in the lower crust and upper mantle following the 2000 June earthquakes causes surface deformation with the same sense of motion as the coseismic displacements (Árnadóttir *et al.* 2005). The post-seismic deformation is mapped as contraction in the areas north of the main shocks and dilatation to the south (Fig. 6a). The maximum shear strain rate is low in the area between Hengill and the 2000 June main shocks, where a change in the direction of the principal strains is also noticeable. This anomaly may be linked to deformation caused by the Hengill inflation (1994–1998) or the 2000 June earthquakes, although the ISNET data lack the spatial and temporal resolution necessary to pinpoint the source. A zone of high maximum shear strain rates is observed along the plate boundary in north Iceland, with a maximum of about 0.4 μstrain yr^{-1} north of Krafla. This maximum appears to be largely due to the eastward motion of station 7384. The motion of this station is most likely influenced by deep magma accumulation north of Krafla (de Zeeuw-van Dalfsen *et al.* 2004) or post-rifting deformation following the 1975–1994 Krafla rifting episode. The TFZ appears as an area of high shear strain rate, although the transform is mostly located offshore.

5 GLACIAL ISOSTATIC ADJUSTMENT

In this section, we examine how much of the observed broad uplift signal could be caused by GIA due to the ongoing melting of Iceland's glaciers. As the present study focuses on presenting the ISNET data and demonstrating how it fits first order deformation processes in Iceland, we will not undertake a detailed GIA investigation. Instead, we will show how well a GIA model comprising simple earth and ice models fits the vertical velocity data. In constraining our GIA models, we are unfortunately not able to include the observed horizontal velocities as they contain much larger contributions from processes other than GIA, such as plate motion and magmatic activity. As noted above, previous studies have focused on the uplift signal around Vatnajökull, Iceland's largest ice cap. Due to the extent of the GPS network in the present study, we can examine the effect of glacial rebound in all of Iceland and we therefore construct a 3-D model which includes melting of four additional glaciers. Langjökull, Hofsjökull and Mýrdalsjökull are the second, third and fourth largest glaciers in Iceland, respectively. We also include Eyjafjallajökull, the sixth largest glacier in Iceland, but due to its proximity to Mýrdalsjökull glacier they are treated as one in our ice model.

5.1 Modelling glacial isostatic adjustment

We model the GIA process using a 3-D, flat Earth, finite element (FE) model of Iceland. The model is 3-D in the sense that we model a rectangular block of the Earth, however, the ice is modelled using a 2-D surface distribution of pressure sources and the earth model itself is 1-D in the sense that rheology and elastic parameters only vary with depth. The element size in the central part of the model is 8×8 km^2 in the horizontal directions and 2 km in the vertical direction. The central block of elements is 272, 416 and 20 km in north-south, east-west and depth, respectively. This block is then gradually transformed into a hemisphere with radius 2700 km. The large radius stabilizes the model and we only extract data from within a radius of 320 km from the centre. We use infinite elements as stress boundary conditions on the outside of the hemisphere.

As we are using the commercial finite element package Abaqus (ABAQUS 2004), we follow the recommendations of Wu (2004) for the use of commercial FE software in GIA applications, approximating the Earth as flat and incompressible, thus neglecting buoyancy and self-gravitation. The two approximations of ignoring self-gravitation and using a flat Earth were shown by Amelung & Wolf (1994) to largely compensate each other. These approximations enable us to write the equation of motion as (Wu 2004)

$$\nabla \cdot \boldsymbol{\sigma} - \rho_0 g_0 \nabla w = 0, \tag{4}$$

where $\boldsymbol{\sigma}$ is the stress tensor, ρ_0 and g_0 the unperturbed density and gravitational acceleration, respectively, and w is the vertical component of the displacement vector. The second term describes the advection of pre-stress, corresponding to the restoring force of isostasy, without which there would be no viscoelastic gravitational relaxation (Wu 2004). We include elastic foundations at all density contrasts in the model in order to account for the pre-stress advection term (Wu 2004). The validity of this modelling approach has been verified by, for example, Wu (1992, 2004), Lund (2005) and Bängtsson & Lund (2008).

5.2 Models of Icelandic glaciation history

Historic sources (e.g. in Thórarinsson 1943; Bergthórsson 1969; Björnsson 1979) indicate that the climate in Iceland became colder after approximately 1200 AD (see also climate reconstructions such as Moberg *et al.* 2005), which promoted growth of the glaciers. Temperatures continued to decrease during the Little Ice Age, which reached its maximum in Iceland around 1800 AD (e.g. McKinzey *et al.* 2005; Bradwell *et al.* 2006). Studies of Icelandic outlet glaciers (Thórarinsson 1943; Björnsson 1979) indicate that although their extent fluctuated somewhat, on average glacier volumes did not change significantly between 1750 and 1890. However, recent simulations of the evolution of Vatnajökull and Langjökull using mass balance measurements and meteorological data suggests that the larger glaciers may have continued to grow until the early 19th century (Flowers *et al.* 2005, 2007).

The Vatnajökull ice cap is Iceland's largest glacier and by far the best studied of the Icelandic glaciers. In 1890, Vatnajökull is inferred to have had an areal extent of approximately 8600 km^2 (Pagli *et al.* 2007a). Since 1890 glaciers in Iceland have been generally retreating (Thórarinsson 1943; Björnsson 1979) and today Vatnajökull covers an area of about 8100 km^2 and has a maximum thickness of approximately 900 m (e.g. Björnsson *et al.* 2002). Pagli *et al.* (2007a) report that the estimate for the volume of ice lost by Vatnajökull between 1890 and 2003 is 435 km^3, a significant

increase from an earlier estimate of 182 km^3 volume loss between 1890 and 1973 (Sigmundsson & Einarsson 1992). Mass balance studies of Vatnajökull show that thinning of the ice occurs at much higher rate at the edge of the ice cap than in the interior (Björnsson *et al.* 1998). Similarly, during periods of colder climate and growth of the ice caps, ice thickness increases more rapidly at the edge of the ice cap due to ice flow from the interior accumulation areas towards the edges.

In studies of GIA the ice history, i.e. the variation in thickness and areal extent of the glaciers with time, is the first order process. Assumptions about the simulated ice history directly influence the modelled rebound rates. Assuming, for example, isostatic equilibrium for Vatnajökull in 1890 (as did e.g. Pagli *et al.* 2007a), will produce an upper limit on the estimated viscosity. This is due to the fact that an earlier Little Ice Age ice accumulation phase would produce subsidence, which would have to be counteracted by lower viscosity in order to fit the rebound velocities we observe today. Because of uncertainties in ice accumulation rates prior to 1890, this study will use a reference ice history which only dates back to 1890, when the crust is assumed to have been in isostatic equilibrium. We will, however, also investigate an ice model reaching back to 900 AD in order to see how a longer ice history affects the viscosity estimate and the resulting rebound velocity field. In addition, we will study how the spatial distribution of melting ice caps influences our results. Previous rebound studies have generally neglected the smaller glaciers of Langjökull, Hofsjökull, Mýrdalsjökull and Eyjafjallajökull. Due to the wide extent of the GPS network in the present study, our ice model will have to include these smaller glaciers, in addition to the large Vatnajökull ice cap, in order to fit the observations.

Following Björnsson *et al.* (1998), our reference ice model will have a zone of high thinning rate around the edge of Vatnajökull. Since the element size in the FE model is relatively large (8×8 km^2), the smaller glaciers will be modelled with uniform ice thickness variations, identical to the higher edge rates on Vatnajökull. This is consistent with the notion that the smaller ice caps will respond more like the outskirts of the larger Vatnajökull than its interior. The areal extent of the glaciers does not change with time in our ice models. This is partly due to the coarseness of the FE grid and partly due to our limited knowledge of prior glacier geometry. The areal extent of the ice caps is modelled on the current extent, but are made larger rather than smaller when defined on the FE mesh, thereby allowing for the maximum areal extent in 1890 (see Table 1). In our models, Vatnajökull has an area of 8768 km^2, which is slightly larger (less than three model elements) than the 8600 km^2 maximum extent in 1890. The error in areal extent increases for the smaller glaciers due to the coarse FE grid. However, the actual 1890 extents of the smaller glaciers are unknown to us. We use the estimated ice volume loss of 435 km^3 since 1890 from Pagli *et al.* (2007a) and also use their average thinning rate of 25 cm of ice (with a density of 917 kg m^{-3}) per year, for the interior of Vatnajökull. As our border between slow interior and fast edge rates, we use the zero annual mass balance contour of Marshall *et al.* (2005, fig. 2f), see Fig. 7. Accounting for the areas of the interior and edge zones, respectively, we find an average thinning rate for the edge zone of 63.4 cm yr^{-1}, very close to the 62 cm yr^{-1} used by Pagli *et al.* (2007a). The faster thinning rate of 63.4 cm yr^{-1} will also be used for the smaller ice caps. For simplicity, our model will not include details in the melting of the glaciers, although measured annual thinning rates are available from recent years (e.g. Björnsson *et al.* 2002). Instead our thinning rates are constant from 1890 to 2004.

Three different ice models are studied below: model (A) includes all five glaciers modelled from 1890 until 2004, with the thinning rates discussed above. Model (B) also starts in 1890 but only includes the Vatnajökull ice cap. For model (C), which contains all five glaciers, we use the ice accumulation estimate of Sigmundsson & Einarsson (1992) of 1265 km^3 from 900 to 1750 AD. We accumulate the ice faster around the edges (24.7 cm yr^{-1}) of Vatnajökull than in the interior (9.75 cm yr^{-1}), with relative accumulation rates based on the relative thinning rates in model (A). For the smaller ice caps, we again use the faster edge rate. From 1750 to 1890, we assume no changes in the ice volumes (as did Sigmundsson & Einarsson 1992) and from 1890 to 2004 we use the model (A).

5.3 Earth models

In this study, we use an earth model based on the simple concept of a flat elastic layer overlying a Maxwell viscoelastic half-space. Our reference model has an incompressible elastic layer with Young's modulus 40 GPa and density 2800 kg m^{-3}. The viscoelastic half-space is also incompressible, with Young's modulus 130 GPa and density 3200 kg m^{-3}. We vary the thickness of the elastic layer and the viscosity of the half-space in order to investigate which combination best fit the observed data. We also examine how the inclusion of a high-viscosity layer below the elastic layer affects the GIA models.

A large number of studies have addressed the thickness and characteristics of the Icelandic crust. From seismological and gravity studies, the crust is inferred to be anomalously thick compared to normal oceanic crust (e.g. Menke *et al.* 1998; Darbyshire *et al.* 2000; Allen *et al.* 2002a; Kaban *et al.* 2002) but crustal thickness is inferred to vary significantly under Iceland, decreasing from approximately 45 km below Vatnajökull to 15 km on the shelf. On average, crustal thickness is approximately 30 km (Allen *et al.* 2002a). Earthquakes usually occur above 10–15 km depth (e.g. Tryggvason *et al.* 2002) but earthquakes at 20 km depth are observed occasionally (e.g. Jakobsdóttir *et al.* 2008). Schmeling & Marquart (2008) review data pertinent to the Icelandic crust, and present models of its formation.

Our earth models are obviously oversimplifications of the rheological structure beneath Iceland as we neither consider spatial variation in crustal thickness nor include a mantle plume. However,

Table 1. Area, thinning rates and volume loss since 1890 used to model the ice history of the Icelandic glaciers.

Glacier	Area (km^2)	Thinning rate (cm yr^{-1})	Volume loss (km^3)
Vatnajökull, total	8768	–	435
Vatnajökull, interior	4544	25.0	129.5
Vatnajökull, rim	4224	63.4	305.5
Langjökull	1152	63.4	83.3
Hofsjökull	1024	63.4	74.0
Mýrdalsjökull + Eyjafjallajökull	896	63.4	64.8

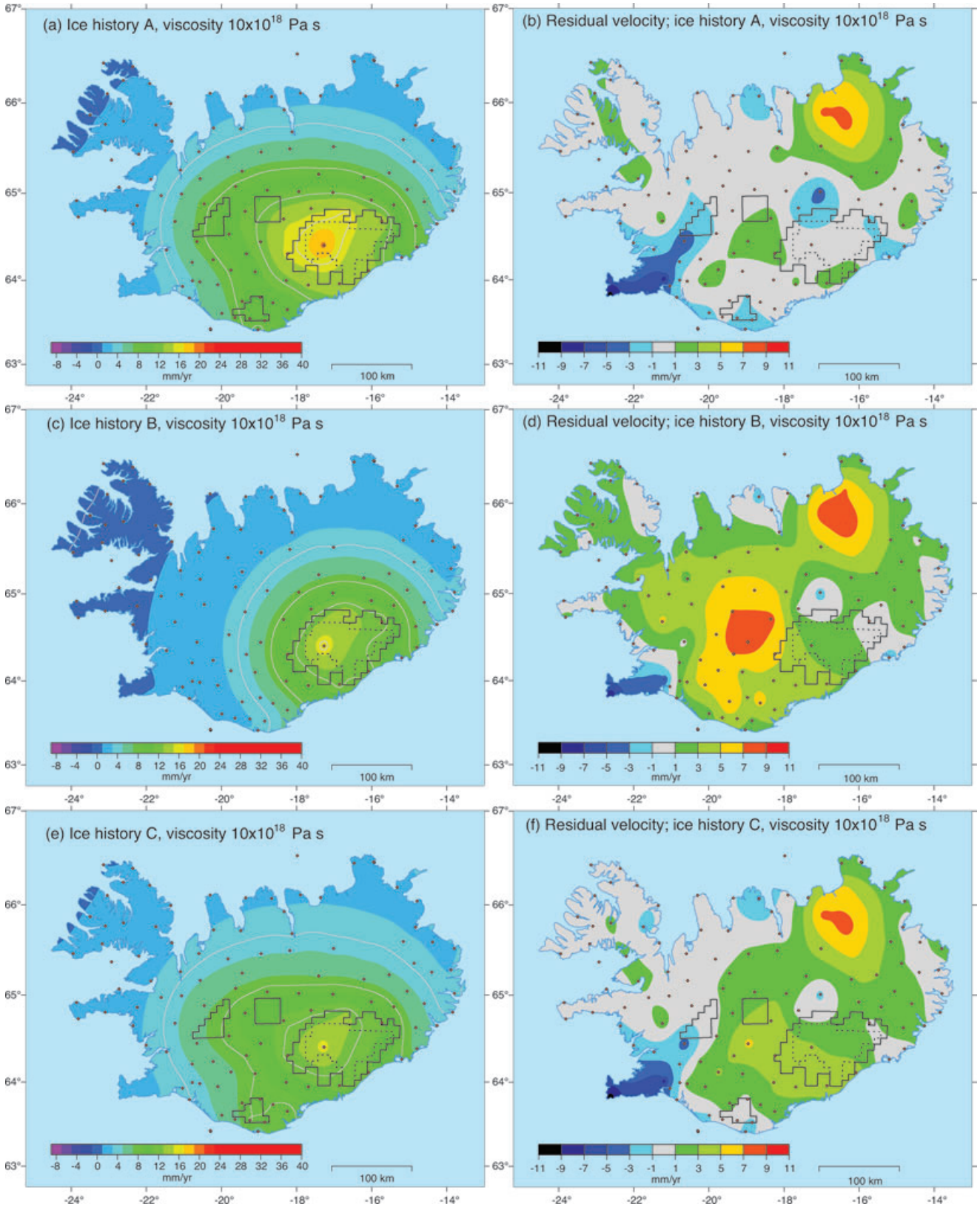

Figure 7. Modelled vertical uplift rates using different ice histories and an earth model with 40-km elastic thickness and a half-space viscosity of 10×10^{18} Pa s. Top row: ice history (A) from equilibrium in 1890 including all four major glaciers. These results are equal to those of our preferred model, see text. Middle row: ice history (B) from equilibrium in 1890 but with only Vatnajökull. Bottom row: ice history (C) with ice accumulation using all four glaciers from 900 to 1750, steady-state from 1750 to 1890 and then deglaciation as in ice history (A). The left column shows the predicted vertical velocities, cf. Fig. 5, and the right column shows residual velocities, data minus model. All maps show the outlines of the modelled glaciers, with Vatnajökull divided into interior and edge areas by a dotted line. Small dots show the locations of the GPS stations included in the χ^2_ν calculation.

these simple models are sufficient to capture the first order GIA signal.

5.4 Modelled uplift rates

The very simple GIA models considered here reproduce the observed broad uplift signal in central Iceland surprisingly well. Fig. 7 shows modelled vertical uplift rates using an earth model with an elastic layer thickness (T_E) of 40 km and a half-space viscosity of 10×10^{18} Pa s. This is the earth model which best fits the observations using ice history (A). The forward model is evaluated at the GPS station locations and the velocity field then interpolated between the stations. We note in Fig. 7(a) that the highest uplift rates are predicted under western Vatnajökull, but that the smaller glaciers seem to broaden the region of moderately high vertical velocities away from Vatnajökull. The difference between the observations and the model is shown in Fig. 7(b). On the large scale, the model captures the broad uplift pattern in the data. Areas of significant misfit in terms of model over-prediction (negative residuals) are the Reykjanes Peninsula, under Mýrdalsjökull and a zone from Kverkfjöll in northern Vatnajökull to the Askja volcano. Similarly, we also have positive residuals where the model underpredicts the data, most noticeably in a broad region around the Krafla volcanic system in northern Iceland and centrally between Vatnajökull and Hofsjökull.

We evaluate the relative merit of our models using a weighted residual sum of squares, $\mathrm{WRSS} = (\mathbf{r}^T \mathbf{r})$, where $\mathbf{r} = (\mathbf{v}^{\mathrm{obs}} - \mathbf{v}^{\mathrm{mod}})/\sigma$. The $\mathbf{v}^{\mathrm{obs}}$ are the observed vertical velocities, σ the associated data uncertainties and $\mathbf{v}^{\mathrm{mod}}$ the model predictions. The level of fit is represented by $\chi^2_\nu = \mathrm{WRSS}/(N - m)$, where N is the number of data, here 109 vertical velocities, and m the number of free model parameters. Since we will vary elastic layer thickness and viscosity in our models, we set $m = 2$. An optimal model has $\chi^2_\nu = 1$, if the data uncertainties are correctly estimated. In these calculations of misfit, we have not included the GPS stations on the Reykjanes Peninsula and its vicinity, as these stations show significant subsidence (Fig. 5) which is inconsistent with glacial rebound (e.g. Fig. 7). We also decided not to include five stations in northern Iceland around the Krafla volcanic region. These stations show rapid uplift which has been attributed to magmatic processes (de Zeeuw-van Dalfsen *et al.* 2004). The residuals at these excluded stations are shown in Figs 7 and 9, but we do not plot the station locations to emphasise that they are not used in the χ^2_ν calculation. As explained in Section 3.2, we also exclude stations SKRO, DYNG and 8434 from both the χ^2_ν calculation and the residual figures in Figs 7 and 9. If included, the combination of all these anomalous stations severely bias the χ^2_ν estimate. Finally, we impose a lower limit ($\sigma = 1.0\ \mathrm{mm\,yr^{-1}}$) on the station uncertainties of the vertical velocities. It is mostly the continuous GPS stations that have lower uncertainty than $1.0\ \mathrm{mm\,yr^{-1}}$, and these are concentrated to south of Mýrdalsjökull and southwestern Iceland. Using the very low uncertainties of the CGPS stations would also unduly bias the misfit estimates. The GIA model in Figs 7(a) and (b) has $\chi^2_\nu = 1.85$.

5.4.1 *The significance of the ice history*

Are the smaller ice caps really necessary in order to reproduce the observations? Figs 7(c) and (d) show the response of the same earth model as in Figs 7(a) and (b) to ice history (B), which only considers Vatnajökull. Comparing the forward model to the result using the (A) ice model in Fig. 7(a), and to the data in Fig. 5, we clearly see how important the contributions from the smaller glaciers are to the uplift pattern away from Vatnajökull. The residuals increase dramatically in west-central Iceland using the (B) ice model compared to the results of the (A) ice. We have used a range of earth models with ice model (B), none of which capture the broad uplift pattern displayed in the data. Comparing the forward models in Figs 7(a) and (c), we also note how the melting of one of the glaciers affects the vertical velocities measured in the vicinity of other glaciers. This implies that rebound studies at, for example, Mýrdalsjökull have to take into account the influence of Vatnajökull, and even studies of western Vatnajökull need to account for the effect of Hofsjökull. In addition, vertical velocity studies for volcano monitoring purposes will clearly have to consider the GIA effect.

We illustrate the effect of a longer glacial history on the uplift rates using ice model (C). With a viscosity on the order of 10×10^{18} Pa s, the relaxation time of the mantle is such that glacier variations before 1890 could be important. Fig. 7 shows, in the lower row, the modelled vertical velocities using ice model (C) and our earth model with 40 km elastic thickness and viscosity 10×10^{18} Pa s. Compared to Fig. 7(a), an ice model with previous ice accumulation smooths the current uplift pattern somewhat, decreasing the vertical velocities under and in the vicinity of Vatnajökull. Inspecting the residual figures, we note that ice model (C) generally produces more positive residuals than ice model (A), for the same viscosity. As discussed previously, this indicates that we need to use a lower viscosity to fit the data equally well with the model (C). Investigating a range of viscosities with ice model (C) and $T_E = 40$ km, a model with viscosity 8×10^{18} Pa s has the lowest χ^2_ν, 1.92. Hence, the difference between the best-fitting viscosities and the best-fitting χ^2_ν, using ice models (A) and (C), is very small. As the glacial history of Iceland from 900 AD until the mid 19th century is still rather uncertain, and seeing that the differences in inferred viscosities are small using ice histories (A) and (C), we will use ice history (A) in our subsequent models, noting that it provides an upper estimate on the viscosity.

5.4.2 *Determining an earth model*

We investigate a range of elastic layer thicknesses and viscosities in order to determine which earth models best fit the data. Fig. 8 shows the results from our simulations in terms of the calculated χ^2_ν and

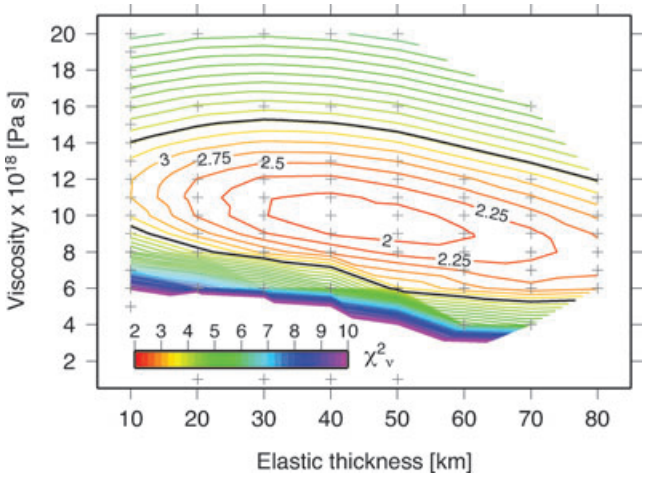

Figure 8. Fit of earth models with varying thickness of the elastic layer (10–80 km) and viscosity of the half-space to the observations using ice history (A). The colour contours show the fit to the data [$\chi^2_\nu = \mathrm{WRSS}/(\mathrm{N\text{-}m})$] and the black line outlines the 90 per cent variance reduction region.

we see that we have a rather narrow minimum in χ^2_ν with respect to viscosity. χ^2_ν increases very rapidly for viscosities below 6–8 $\times$ 10^{18} Pa s, with the threshold viscosity value depending rather weakly on the elastic thickness. Contrary to the viscosity, the thickness of the elastic layer is not well resolved. Models with elastic thickness between 30 and 60 km fit the observed data almost equally well, with the best-fitting model having $T_E = 40$ km, a viscoelastic half-space viscosity of 10×10^{18} Pa s and $\chi^2_\nu = 1.85$, as indicated above. We note a small trade-off between elastic layer thickness and viscosity as the best-fitting model with $T_E = 10$ km has viscosity 11×10^{18} Pa s ($\chi^2_\nu = 3.00$) and the best-fitting model with $T_E = 80$ km has viscosity 8×10^{18} Pa s ($\chi^2_\nu = 2.39$).

In Fig. 9, we illustrate the influence of viscosity and elastic layer thickness on the modelled uplift rates. Two models with 40-km thick elastic layers are shown in Figs 9(a,b) and (c,d), with viscosities 6×10^{18} and 20×10^{18} Pa s, respectively. A model with viscosity 10×10^{18} Pa s but with an elastic thickness of only 10 km is included in Figs 9(e) and (f). We see in the forward models that the large scale uplift pattern and the uplift velocities away from the glaciers vary rather slowly with viscosity. On the contrary, velocities in the vicinity of, and under, the ice caps are very sensitive to the assumed viscosity. This is especially true for the large Vatnajökull ice cap and emphasises the need for more GPS stations on glacier nunataks. We also note that a decreased elastic thickness, compare Figs 7(a) and 9(e), brings out more detail (high-frequency content) in the vertical velocities and shows higher rates under, and in the vicinity of, Vatnajökull. Comparing the models to the observed data, we see that the residual pattern described above is persistent in spite of variations in the viscosity and elastic thickness. The Reykjanes Peninsula, WVZ, Mýrdalsjökull and the region north of Vatnajökull have negative residuals and central Iceland and the Krafla volcanic system have positive residuals.

The best-fitting elastic thicknesses we estimate in our simple rheological models are slightly thicker than the recent seismological and gravity derived estimates of crustal thickness in Iceland discussed above. As the elastic thickness in GIA models is frequently interpreted as the mechanical thickness of the lithosphere, our results indicate a thin mantle lithosphere under the Icelandic crust. However, the tectonic setting of Iceland atop a mantle plume and thermal models of the island (e.g. Kaban *et al.* 2002) suggest that the lower crust and upper mantle are ductile. We therefore investigate how models with a ductile lower lithosphere affect the simulated vertical velocities. Basing our models on the 40-km thick elastic layer model, we use a 10-km thick elastic layer and a 30-km viscoelastic layer, representing the upper and lower lithosphere, respectively, atop a viscoelastic half-space. We do not attempt here to invert for a best fit model, we simply show how the inclusion of a viscoelastic lower lithosphere affects the results. The lower lithospheric layer is modelled as an incompressible material with Young's modulus 70 GPa, density 3000 kg m^{-3} and varying viscosity. Fig. 10 shows the χ^2_ν distribution when the viscosity of the lower lithosphere is increased from 1×10^{19} to 1×10^{24} Pa s, while the viscoelastic half-space has a constant viscosity of 1×10^{19} Pa s. The models thus effectively go from a 10-km elastic layer on a viscoelastic half-space to a 40-km elastic layer on a viscoelastic half-space. We see in Fig. 10 that for the ISNET station geometry and the 114-yr time span of our GIA model, the lower lithospheric layer effectively acts elastically for viscosities of 1×10^{20} Pa s or higher. The rather thick elastic layer estimated above is therefore not strictly necessary but can be subdivided into an elastic layer and a layer with a viscosity that is at least one order of magnitude higher than the viscosity of the half-space below. The χ^2_ν for the model with a 1×10^{20} Pa s lower lithosphere is 1.96 and it is 1.85 for the models with viscosity larger than 1×10^{21} Pa s. We recall that the $T_E = 40$ km model with half-space viscosity 1×10^{19} Pa s has $\chi^2_\nu = 1.85$.

We note that although the intermediate viscoelastic layer uses different elastic parameters (Young's modulus and density) than the upper elastic layer and the viscoelastic half-space, these differences do not influence the model response significantly. For example, the model in Fig. 7(a) with a 40-km elastic layer on top of a viscoelastic half-space has $\chi^2_\nu = 1.85$, exactly the same as a model with a 10-km elastic layer, a 30-km intermediate viscoelastic layer with viscosity 1×10^{21} Pa s on a viscoelastic half-space.

As discussed above, Fig. 8 indicates fairly tight constraints on the admissible range of viscosities but a wide range of elastic thicknesses. We use the variance reduction, VR $= 100[1 - \chi^2_\nu(\text{opt})/\chi^2_\nu(\text{null})]$ where $\chi^2_\nu(\text{opt})$ is for the optimal model and $\chi^2_\nu(\text{null})$ is for no model, to define a range of well fitting models. The best-fitting model, with $T_E = 40$ km and viscosity 10×10^{18} Pa s, reduces the variance by 94.7 per cent and the model with a 1×10^{20} Pa s viscoelastic lower lithosphere has VR = 94.4 per cent. The difference in variance reduction between these models is insignificant and we select the lower lithospheric model, i.e. $T_E =$ 10 km, a 30 km 1×10^{20} Pa s viscoelastic lower lithosphere and a mantle with viscosity 1×10^{19} Pa s, as our preferred model due to its similarities to models based on seismology, density and heat flow. The vertical velocities predicted by this model, and hence the vertical residuals, are almost identical to those in Figs 7(a) and (b).

We are not able to properly define a range of well-fitting models as we have not run all combinations of models and parameters. From the models we have run, e.g. Figs 8 and 10, and using a variance reduction in the range 90–95 per cent (shown by the thick black line in Fig. 8), we suggest that half-space viscosities in the range of 6–15 $\times$ 10^{18} Pa s predict vertical rates in reasonable agreement with the data for elastic thickness variations from 10 to 80 km, with or without a ductile lower lithospheric layer with viscosity higher than that of the mantle. Obviously, not all viscosities can be combined with all elastic thicknesses.

6 PLATE BOUNDARY DEFORMATION

6.1 Plate boundary models

Several studies have described the observed deformation in southern Iceland in terms of kinematic models (Hreinsdóttir *et al.* 2001; LaFemina *et al.* 2005; Árnadóttir *et al.* 2006; Keiding *et al.* 2008). In this section, we extend a kinematic model applied to SW Iceland by Árnadóttir *et al.* (2006) to the whole island, in order to explain the plate spreading signal we observe with the ISNET measurements. Our primary goal here is to estimate model parameters that describe the plate spreading, which is mainly manifested by horizontal motion. The modelling of crustal deformation in Iceland is, however, not a simple task because of the complex geometry of the plate boundary, with the spreading accommodated by several overlapping volcanic fissure swarms, as well as multiple potential sources of deformation due to earthquakes and active volcanoes. The ISNET station spacing and lack of temporal resolution limit our ability to accurately resolve the location and volume changes of possible magma sources. In addition, the vertical GPS velocities are significantly affected by GIA, as described in the previous section. We therefore correct the observed vertical GPS velocities for the glacial rebound signal using the optimal model from the

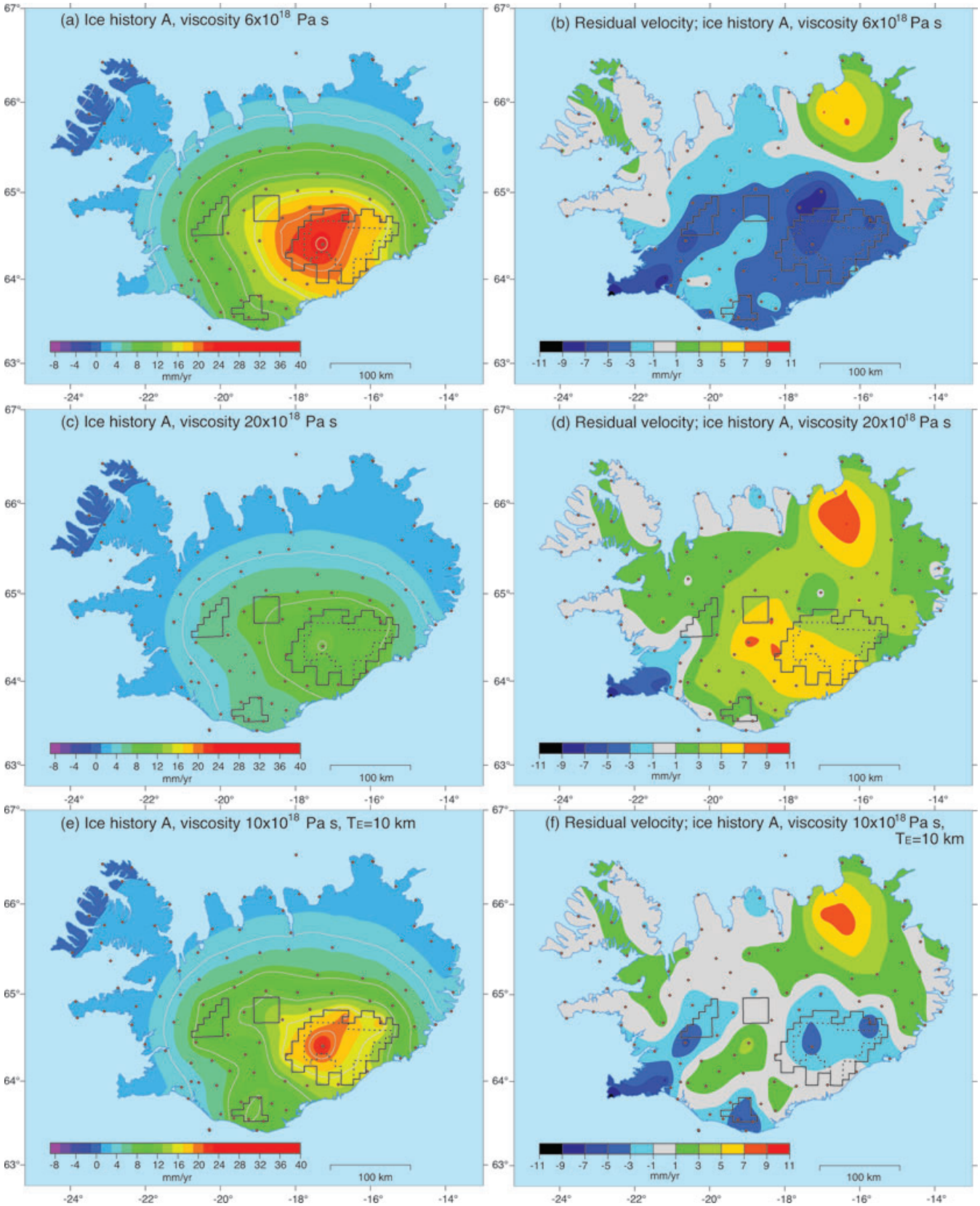

Figure 9. Modelled vertical uplift rates using different earth models and ice history (A). All the models have an elastic layer of thickness T_E underlain by a viscoelastic half-space. Top row: $T_E = 40$ km and viscosity 6×10^{18} Pa s. Middle row: $T_E = 40$ km and viscosity 20×10^{18} Pa s. Bottom row: T_E=10 km and viscosity 10×10^{18} Pa s. The left column shows the predicted vertical velocities, cf. Fig. 5, and the right column shows residual velocities, data minus model. All maps show the outlines of the modelled glaciers, with Vatnajökull divided into interior and edge areas by a dotted line. Small dots show the locations of the GPS stations included in the χ^2_ν calculation.

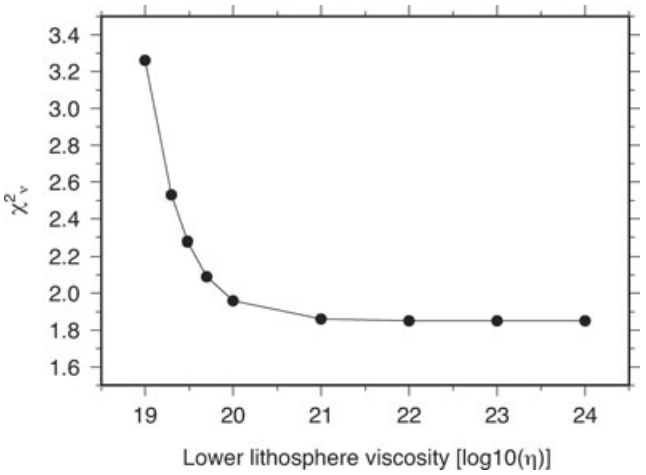

Figure 10. Fit to the observations of earth models with a 10-km elastic upper lithosphere and a 30-km viscoelastic lower lithosphere with varying viscosity overlying a viscoelastic half-space with viscosity of 10×10^{18} Pa s. All models use ice history (A).

previous section (see Table S3, Supporting Information), but also down weight the vertical velocities by increasing the data uncertainty. We exclude stations that may be affected by local deformation (see Table S2, Supporting Information). In order to increase our model resolution, we include velocities at several CGPS stations in Iceland, although the time series for these stations are shorter than the time interval spanned by the ISNET observations.

In our kinematic models, we assume that the Earth is an elastic half-space, and represent the plate boundary with a series of vertical dislocations. We use trial-and-error to obtain the simplest geometry of the plate boundary through Iceland. We refer to the different segments of the plate boundary, using the following abbreviations: RR denotes the offshore Reykjanes Ridge, RPW is the western part of the Reykjanes Peninsula, RP represents the central and eastern part of the Reykjanes Peninsula, SISZ, WVZ, EVZ, NVZ (defined in the previous pages) and KR denotes the Kolbeinsey ridge. We include two transforms in the TFZ, as the deformation is possibly accommodated both on the HFF and the GL (Geirsson *et al.* 2006). We use epicentral locations of microseismicity as a guide in determining the location and orientation of the dislocations representing these offshore segments. From the relative plate motion and the more northerly orientation of the GL, we allow right–lateral slip on both segments as well as opening on the GL. Our model also includes six Mogi point sources representing magma sources below the central volcanoes Hekla, Katla, Grímsvötn, Bárdarbunga and Askja. We also include a source located north of Krafla as suggested in the study of de Zeeuw-van Dalfsen *et al.* (2004).

We estimate the locking depths and rates of opening and/or strike-slip motion on the dislocations, as well as the depth and volume change for the point sources, to best match the GPS station velocities. The model parameters are a non-linear function of the surface velocity data. We therefore apply a non-linear optimization scheme that uses a simulated annealing search algorithm, followed by a derivative based method (e.g. Cervelli *et al.* 2001) to estimate the best fit model parameters, by minimizing a similar weighted residual sum of squares, WRSS, as in the GIA modelling. Here $\mathbf{v}^{\rm obs}$ is a vector with the velocities in east, north and vertical. The fit of the model to the data is assessed with χ^2_ν, calculated as above. Following Árnadóttir *et al.* (2006), we determine an optimal model using all the data and a range of possible model parameters by applying a bootstrap method, whereby the model parameters are obtained by optimization of a resampled set of 125 GPS station velocities ($N = 375$). The resampled data set contains the three components of the velocity at randomly selected stations, where some stations may be sampled more than once and others not included. This procedure is repeated many times, producing a large number of models. The resulting individual model parameters are sorted by numerical values, and the 95 per cent confidence limit estimated by discarding the largest and smallest 2.5 per cent of the values.

The GPS station velocities predicted by the optimal model ($\chi^2_\nu = 1.74$) are shown in Fig. 11. The observed velocities are now plotted as averages of the velocities relative to stable North America and Eurasia (Figs 3 and 4), hence representing a ridge-centred reference frame. The optimal model parameters, as well as the mean values and confidence intervals estimated by the bootstrap procedure are given in Tables 2 and 3. Many of the model parameters have wide bounds, indicating that their resolution is limited by trade-off between the locking depths and slip rates and/or opening on the dislocations, as well as the depth and volume change for the Mogi point sources. We fix the slip rate on the RPW to 20 mm yr^{-1} in all our models, as otherwise this segment has an unreasonably high slip rate (>30 mm yr^{-1}). The high slip rate on the RPW and suggestion of contraction, rather than opening on this model segment, is most likely due to the high rate of subsidence observed at the western most station on the Reykjanes Peninsula. Adding a point source representing the subsidence at Svartsengi did not improve the model fit nor explain the contraction on the RPW segment. We therefore do not include a Mogi source at Svartsengi in the plate boundary model. Most notably, our optimal model indicates a significantly higher spreading rate on the NVZ (23 ± 2 mm yr^{-1}) than the expected far field rate ($\sim$20 mm yr^{-1}). Overall, the locking depths range between 5 and 15 km, with greater locking depths indicated on the GL and KR. The depths of the point sources appear to be >5 km, in general agreement with results from prior studies, although the uncertainties on the point source model parameters are too large to render them meaningful.

The horizontal residual velocities, after subtracting the velocities predicted by the plate boundary model from the observations, are shown in Fig. 11(b) (blue arrows). The azimuth and magnitude of the residual plate boundary model velocities in east Iceland show a systematic radial pattern away from Vatnajökull. These residual velocities show a remarkable agreement to the ISNET velocities in the stable Eurasia reference frame, as shown in Fig. 4. This indicates that the horizontal residual model velocities are due to processes other than plate spreading and volcano deformation, such as the horizontal component of the GIA signal, at least at stations close to the glacier.

6.2 Plate boundary modelling results

A detailed comparison of our estimated model parameters and previous studies is difficult since these studies use data from different time intervals and denser more localized networks, thus considering a smaller portion of the plate boundary than we do here. In addition, temporal variations in the rate of deformation that we are unable to resolve with the ISNET observations may affect our model estimates. As explained in the introduction, the active volcanoes have displayed a range of magmatic activity during the time spanned by the ISNET measurements. For example, Hekla erupted in 2000, Gjálp in 1996 and Grímsvötn in 1998. The ISNET

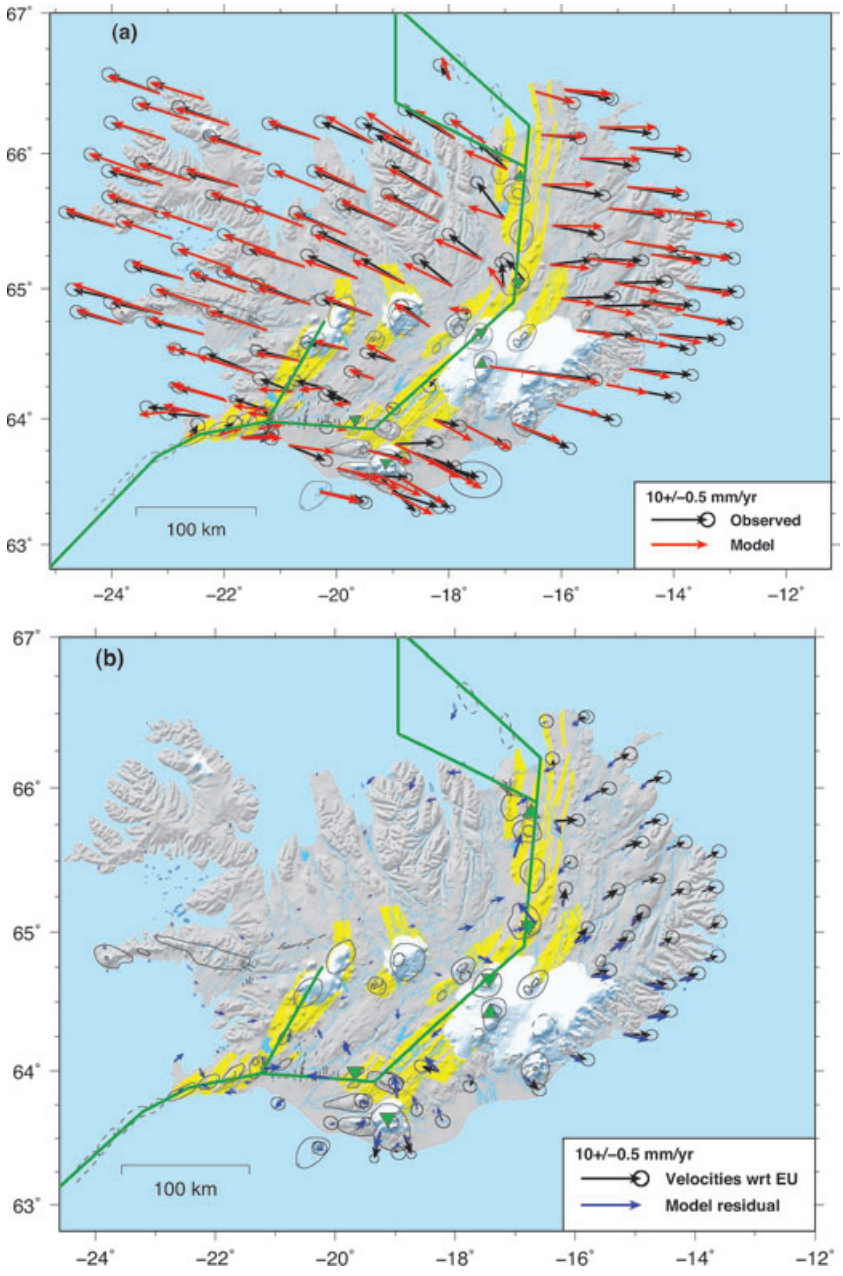

Figure 11. (a) Predicted horizontal velocities from the optimal plate boundary model (red arrows) compared to observed velocities in a ridge-centred reference frame (black arrows with 95 per cent confidence ellipses). (b) Residual velocities (blue arrows), i.e. observed velocities minus the optimal plate boundary model predictions, compared to velocities in east Iceland relative to stable Eurasia (black arrows with 95 per cent confidence ellipses). The model parameters are given in Tables 2 and 3. The green lines represent the surface projection of the plate boundary dislocation models. The inflating point sources are indicated with green triangles and deflating sources with inverted triangles.

observations therefore include periods of inflation prior to the eruptions, rapid coeruptive deflation and most likely inflation following the eruptions. Our estimate for the Mogi source volumes in this study are thus averages for the 11-yr time interval, and do not represent the short-term activity at these volcanoes. Many of the volcanoes are subglacial, and although we attempt to correct for the vertical GIA signal, horizontal deformation due to the load decrease is not accounted for, which may affect our parameter estimates. The deformation in central Iceland is influenced by several magmatic episodes at the active central volcanoes Bárdarbunga and Grímsvötn, as well as GIA and plate spreading. Furthermore, these volcanoes are located beneath Vatnajökull ice cap, limiting the number of geodetic stations that can be used to study the surface deformation due to magma accumulation, eruptions or intrusive activity. As the ISNET network is not very dense, we fix the location of the point sources representing the volcanoes and estimate only the source depths and volume changes (Table 3). In general, the optimal model parameters agree with the mean from the bootstrap estimates. Small discrepancies are, however, noted that are most likely due to the optimal solution depending heavily on velocities from a single station. Due to the large uncertainties of the model parameters and the long time-span of the ISNET data, we will not discuss our estimates of the magma sources here. In the following, we compare the deep slip rates and locking depths we estimate on the

Table 2. Plate boundary dislocation model parameters.

Segment	D (km)	SS (mm yr^{-1})	OP (mm yr^{-1})
RR	9.4	–	12.5
	8.1 (5.5; 9.9)	–	12.2 (5.8; 22.2)
RPW	7.1	20*	−14.1
	7.0 (5.0; 9.8)	20*	−13.6 (−28.4; −7.0)
RP	5.3	23.1	10.6
	5.1 (5.0; 6.5)	23.0 (19.8; 26.6)	10.0 (9.0; 12.0)
SISZ	6.5	17.5	–
	7.2 (5.1; 9.9)	17.9 (14.6; 21.3)	–
WVZ	5.2	–	9.5
	5.5 (5.0; 6.5)	–	9.8 (7.3; 12.4)
EVZ	8.9	–	21.7
	8.7 (5.8; 10.0)	–	20.9 (18.5; 23.1)
NVZ	4.9	–	23.1
	5.1 (3.2; 7.0)	–	23.0 (21.4; 24.7)
GL	13.8	−18.1	1.0
	12.2 (4.0; 14.9)	−16.6 (−21.9; −9.0)	1.0 (−3.0; 4.9)
HFF	4.7	−1.0	–
	7.5 (3.1; 14.4)	−1.3 (−8.0; 4.8)	–
KR	14.5	–	16.0
	12.5 (4.5; 14.9)	–	17.2 (13.2; 21.0)

Dislocation parameters for the best fit plate boundary model from non-linear optimization using all the data. The results from the bootstrap calculations are given below the optimal parameter as the mean values with the lower and upper bounds in parenthesis. The model parameters we estimate are the locking depth (D), the deep slip rate (SS) where a positive number indicates left-lateral slip, and the rate of opening (OP). A* indicates that the parameter was fixed and a dash means that the parameter was not estimated. The Mogi model parameters are given in Table 3.

Table 3. Mogi point sources.

Location	Latitude (°N)	Longitude (°W)	Depth (km)	ΔV ($\times 10^6$ m^3 yr^{-1})
Askja[a]	65.044	16.769	9.5	−4.0
			6.0 (1.2; 16.1)	−2.4 (−6.9; −0.2)
Bárdarbunga[b]	64.67	17.43	7.6	−8.4
			5.3 (1.1; 16.5)	−5.5 (−9.8; −0.1)
Grímsvötn*	64.423	17.419	7.6	9.5
			7.3 (2.0; 13.4)	9.2 (6.1; 10.0)
Hekla[c]	63.994	19.671	15.5	−0.1
			14.3 (3.0; 19.8)	−0.3 (−2.7; 0.0)
Katla[c]	63.654	19.122	14.0	−0.1
			14.7 (3.5; 19.9)	−0.3 (−1.8; 0.0)
Krafla N[d]	65.83	16.73	14.0	4.7
			11.4 (1.6; 19.6)	5.3 (0.3; 15.6)

Mogi source parameters for the optimal plate boundary model. The mean values estimated from the bootstrap calculations are also given with the bounds (95 per cent confidence limits) in parenthesis. The depth is the source depth and ΔV is the estimated volume change. Location is the geographic location of the source. All but one of the magma source locations are fixed using results from prior studies: [a] Pagli *et al.* (2006), [b]Pagli *et al.* (2007b), [c]Sturkell (personal communication, 2008), [d]de Zeeuw-van Dalfsen *et al.* (2004), *estimated in this study.

different segments of our plate boundary model (Table 2) to previous studies.

We observe locking depths ranging from 5 to 10 km in south Iceland. The resolution is, however, hampered by the small number of ISNET stations on the Reykjanes Peninsula. Our bootstrap model estimations (95 per cent confidence intervals) indicate a similar range of locking depths (5–7 km) on the peninsula, as 95 per cent confidence intervals obtained by previous studies (5–12 km) (Hreinsdóttir *et al.* 2001; Árnadóttir *et al.* 2006; Keiding *et al.* 2008). The slip rates we find are, however, rather high (20–27 mm yr^{-1}) although this range overlaps with prior estimates (13–24 mm yr^{-1}). As Árnadóttir *et al.* (2006) and Keiding *et al.* (2008), we find a significant rate of opening (>5 mm yr^{-1}) on the RP. In the SISZ, our slip rate (18 ± 3 mm yr^{-1}) is better constrained than the estimate from Árnadóttir *et al.* (2006) (19 ± 10 mm yr^{-1}), probably due to the wide aperture of the ISNET network. Our estimated locking depth (7^{-2}_{+3} km) appears to be shallower, although near the lower bounds obtained by Árnadóttir *et al.* (2006) for 1992–2000 (15^{-5}_{+8} km). The locking depth obtained in this study may be biased towards a shallower depth due to post-seismic deformation following the 2000 June earthquakes. A locking depth of about 5 km on the RP and ∼10 km in the SISZ agrees with the general increase from west to east in the maximum depth of earthquakes in the area (5–13 km) (Tryggvason *et al.* 2002; Árnadóttir *et al.* 2006).

The range of locking depths we obtain in the EVZ (6–10 km) is significantly deeper than the 3 ± 1 km depth LaFemina *et al.* (2005) obtained from a 2-D model of a profile across the central part of the EVZ and WVZ, whereas our locking depth for the WVZ of 5–7 km is within the uncertainty of their estimate (4^{-1}_{+2} km). We find a rate of opening of 21 ± 2 mm yr^{-1} across the EVZ and 10 ± 3 mm yr^{-1} on the WVZ. The lower bounds of the rates we determine on these segments are comparable to the rates found by LaFemina *et al.* (2005), i.e. 19.0 ± 1 mm yr^{-1} (northern EVZ) and 7.0 ± 0.4 mm yr^{-1} (WVZ). We were not able to resolve variation in spreading rates along the strike of the two rift zones, previously inferred by LaFemina *et al.* (2005). Low strain rates in the area north of Langjökull, however, support a decrease in spreading rates towards the northern end of the WVZ. The assumption of constant rates of opening may bias our estimates as such lateral variation will affect the resulting model parameters due to the trade-off between the locking depth and the slip rate. In general, a model with shallower locking depth and lower slip rates can produce surface deformation that is similar to a deeper locking depth and higher slip rates. The ISNET network includes stations far away from the rift zones, which should help constrain the deep slip rates, but the network is less dense across the deforming zone than in the study by LaFemina *et al.* (2005), which affects our ability to resolve the locking depth and spatial variation in the slip rates. Combining data from the dense network in south Iceland with the more distant stations in the ISNET network may help resolve this apparent discrepancy in our results. The low uncertainties in model estimates from LaFemina *et al.* (2005) stem from the 2-D model they apply which does not account for the trade-off between the different model parameters (other than the locking depth and deep slip rate), resulting in a narrower range of their estimates than indicated by the bootstrap method we apply. We also explored models including an E–W segment representing the MIB in central Iceland. Adding this segment did not improve the fit to the data, and very little motion (<3 mm yr^{-1} of strike-slip and/or opening) was indicated. We therefore do not include the MIB in our optimal plate boundary model.

We find an elevated rate of opening (23 ± 2 mm yr^{-1}) and a shallow locking depth (5 ± 2 km) for the NVZ segment. Significantly higher rates of opening (34 mm yr^{-1}) are suggested by de

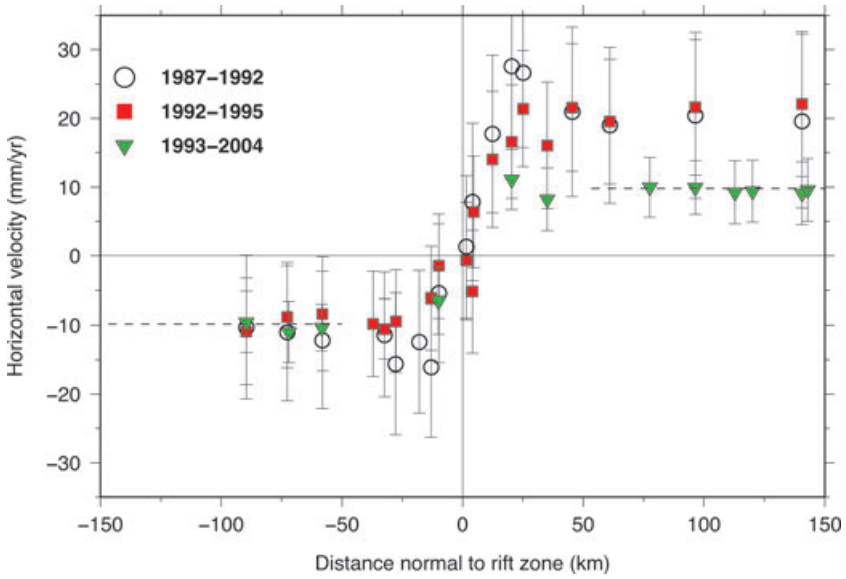

Figure 12. Horizontal GPS station velocities along a ∼50-km wide NNW–SSE profile shown in Fig. 2 oriented perpendicular to the trend of the Krafla fissure swarm (N15°E). The velocities show the spreading across northeast Iceland for the time intervals 1987–1992 (open circles), 1992–1995 (red squares) and 1993–2004 (green inverted triangles). The dashed line shows the ±9.8 mm yr^{-1} of relative motion predicted by plate motion models. The error bars indicate the 68 per cent confidence interval. The velocities for 1987–1992 and 1992–1995 are from Völksen (2000).

Zeeuw-van Dalfsen *et al.* (2004), in a study using InSAR data spanning 1993–1999, assuming a locking depth of 4.6 km. Early GPS observations in north Iceland indicate high rates of extension across the NVZ during 1987–1990 (56 mm yr^{-1}), 1987–1992 (about 40 mm yr^{-1}) and 1992–1995 (∼30 mm yr^{-1}) (Foulger *et al.* 1992; Hofton & Foulger 1996; Völksen 2000). The GPS velocities have been interpreted as post-rifting deformation following the Krafla Fires (1975–1984) (e.g. Foulger *et al.* 1992; Hofton & Foulger 1996; Pollitz & Sacks 1996). Fig. 12 summarises the horizontal velocities in a ∼50 km wide NW–SE profile in north Iceland determined from the earlier GPS observations and the ISNET measurements. The location of the profile area is drawn in Fig. 2. Fig. 12 clearly demonstrates that the elevated rate of extension across the Krafla fissure swarm estimated from the earlier studies is no longer observed and the ISNET velocities are in good agreement with the expected far-field plate motion in northern Iceland. We therefore conclude that the ISNET velocities do not indicate a significant post-rifting transient across north Iceland, as inferred from early GPS studies, and any remaining post-rifting signal could be confined to the Krafla fissure swarm, where we lack spatial resolution. We do not apply viscoelastic models to explore further the post-rifting deformation in north Iceland, since there is no temporal resolution in the ISNET data, and the time spanned by the ISNET observations is quite long.

Our plate boundary model includes the GL and the HFF. As expected, our model parameters in this area are rather poorly constrained. We estimate locking depths of 4–15 km and slip rates of 9–22 mm yr^{-1}, as well as a small component of opening (1 ± 4 mm yr^{-1}) on the GL. Our models, however, indicate very low slip rates on the HFF (<5 mm yr^{-1}). This does not agree with the conclusion of Geirsson *et al.* (2006), who interpreted relative velocities of three CGPS stations in the area (RHOF, ARHO and AKUR), as indication of similar slip rates on the GL and the HFF. From relative relocations of microseismicity Rögnvaldsson *et al.* (1998) report the maximum depth of earthquakes on the HFF increasing from about 5 km near the Kolbeinsey ridge to about 10-km depth below the eastern part of the fault. Our models, however, indicate a shallower locking depth for the HFF (∼5 km) than on the GL and KR (∼15 km), although none of these estimates are well resolved.

Further improvements in modelling the plate boundary deformation in Iceland require including data from denser networks in the deforming areas, thereby increasing the spatial and temporal resolution in order to be able to correct for, or simultaneously estimate, deformation due to active volcanos, glacial isostatic rebound and other local signals which currently affect our model estimates.

7 DISCUSSION

7.1 Glacial isostatic adjustment models

Simulations of the Earth's response to glacial loading and unloading requires knowledge of both the glacial history and the structure and rheology of the Earth. In this section, we discuss how the simplicity of our GIA models may influence our inferences on the rheology below Iceland and compare our results to estimates from other studies.

7.1.1 Other potential sources of uplift

In this study, we have considered glacial rebound (using the four largest glaciers in Iceland plus Eyjafjallajökull, the sixth largest glacier) as the only source of uplift when explaining the observed vertical velocities. Here, we discuss other processes that may contribute to the observed uplift and their potential impact on our results. In general, unaccounted for processes that produce a large-scale uplift signal implies that we will compare our GIA models to observations which are larger than those produced by the GIA process alone. This will bias our estimates of mantle viscosity towards too low values. Processes producing more local uplift will add specific areas of large residuals in our analysis.

One obvious source of uplift is additional glaciers and long lasting snow fields. The fifth largest glacier in Iceland, Drangajökull, is located on the northernmost peninsula in the western fjords

(Fig. 1). We do not include this glacier in our models as the ice history is poorly known and as Fig. 5 does not show a significant localized vertical velocity anomaly in the area. In addition, Drangajökull is melting more slowly than the glaciers in south Iceland. Smaller glaciers with an area larger than 5 km^2 are all located in the vicinity of the four largest glaciers, except the Snæfellsjökull glacier on the western tip of the Snæfellsnes Peninsula. Since we deliberately have larger modelled glacier areas than the current areal extent of the glaciers, as discussed in Section 5.2, the omission of the smaller glaciers should be compensated for. There are a number of small glaciers on the Tröllaskagi Peninsula (Fig. 1) (Björnsson & Pálsson 2008), covering in total almost the same area as the Drangajökull glacier but with much smaller volume. The data do, however, not indicate any local contributions to the vertical velocities on Tröllaskagi. Geirsson *et al.* (2006) estimate the snow load in winter as ∼1 m (water equivalent) in central Iceland. Most of the snow in central Iceland melts in summer, inducing a seasonal loading cycle rather than a long-term loading/deloading signal. Long-term trends in snow load in Iceland are not well documented but presumably follow the accumulation and melting pattern of the glaciers, albeit with a more rapid response. It is therefore likely that smaller ice and snow fields completely disappeared during the previous warm period in Iceland, 1920–1965 (e.g. Hanna *et al.* 2004), and then regrew during the ensuing cold period, indicating that their average influence on GIA during the latter part of the 20th century is very small.

Global sea-level has been rising 195 mm between 1870 and 2004 (Church & White 2006), loading the Icelandic shelf by an average of 1.46-mm water per year. Using a simple model, where we load our preferred earth model with this sea-level rise outside the coastline of Iceland, shows that sea-level rise induces subsidence of the island, on the level of less than 0.2 mm yr^{-1}. This result could perhaps change if we used a model with the proper sea-floor topography, including the continental slope. However, even if such a model would reverse the sense of motion, inducing uplift centrally on Iceland, the magnitude of the signal is much smaller than the uncertainties in the GPS measurements.

Erosion is another potential source of uplift. The ice caps erode and transport large amounts of material from their catchment areas into the glacially fed rivers. Gíslason (2008) reports both glacial erosion rates and estimates of subaerial erosion in Iceland. Mýrdalsjökull has the highest erosion rate of all glaciers, approximately 12 000 tonnes $km^{-2}\,yr^{-1}$. This is equivalent to 118 Pa yr^{-1} pressure release. The corresponding pressure release due to deglaciation is 5.67 kPa yr^{-1}, making the erosion rate 2.1 per cent by weight of the deglaciation rate. Less erosion is reported at the other glaciers, and the corresponding ratios of erosion to deglaciation rates therefore also smaller. Flowers *et al.* (2007) measured sedimentation from Langjökull into Hvítárvatn and found a rate higher than that of Gíslason (2008), but still corresponding to less than 1 per cent by weight of the deglaciation rate. The subaerial erosion rates in Iceland are estimated to be the highest in the area around Mýrdalsjökull, with 100–200 tonnes $km^{-2}\,yr^{-1}$, whereas the rates in central Iceland are 20–50 tonnes $km^{-2}\,yr^{-1}$ (Gíslason 2008). These rates are equivalent to 1–2 and 0.2–0.5 Pa yr^{-1} pressure release, respectively. These studies imply that both glacial and subaerial erosion rates are low compared to the deglaciation rates and can be ignored for our purposes.

Iceland sits atop the Mid-Atlantic ridge because of the mantle plume. Could the plume itself contribute to the observed uplift? The observed vertical velocities of up to 2 cm yr^{-1} can of course not have been sustained for a very long time period, even with significant secondary lateral crustal flow. A rapidly pulsating plume (e.g. Ito 2001) could potentially provide significant vertical motion over a limited time. A rough estimate of the vertical surface velocities produced by one such dynamic, pulsating plume model shows, however, that the resulting uplift rate is on the order of 0.5–1 mm yr^{-1} (H. Schmeling, 2007, personal communication). This is on the level of the uncertainty in the GPS measurements, implying that plume related surface motion may be very difficult to detect and probably contributes very little to the observed uplift. Magmatic sources closer to the surface of the Earth, such as magma chambers and eruptions, have large effects on the GPS measurements in Iceland and will be discussed in Section 7.2.

7.1.2 The ice model

The ice history, i.e. the temporal variation in ice thickness and areal extent, is of utmost importance for a correct simulation of the GIA process. An illustration of the significance of the ice load is provided by the comparison of our results with those of Fleming *et al.* (2007). They base their ice models on the 182 km^3 of ice loss between 1890 and 1973, 2.19 $km^3\,yr^{-1}$, estimated by Sigmundsson & Einarsson (1992), which is less than 60 per cent of the current estimate, 435 km^3 between 1890 and 2003, 3.85 $km^3\,yr^{-1}$ (Pagli *et al.* 2007a), used in this study. In spite of slight differences in the earth models, Fleming *et al.* (2007) use a higher viscosity mantle below their asthenosphere, the order of magnitude difference between their inferred viscosities $1–2 \times 10^{18}$ Pa s and our $6–15 \times 10^{18}$ Pa s, is most likely due to this difference in the deglaciation rates.

In this study, we used a constant thinning rate from 1890 to 2004, as well as identical deglaciation rates for the smaller ice caps and the outskirts of Vatnajökull. These are simplifications, as we know that the glacier retreat rates have varied significantly during the 20th century (Thórarinsson 1943; Björnsson 1979; Björnsson *et al.* 2002). Recent variations in deglaciation rates can be potentially important, especially when comparing rebound data collected in different time periods as we do here with the ISNET data and the continuous GPS data. Björnsson *et al.* (2002) indicate that there was a change at Vatnajökull from slight accumulation to rapid deglaciation in the mid 1990s, which is during the ISNET time period but before the CGPS era. Rapid variations in deglaciation rates will be most noticeable close to the glaciers, so observation points near the glacier rims, or outlet glaciers, are likely to be most affected. This could be applicable to some of the stations very close to Mýrdalsjökull and Vatnajökull. In addition, Mýrdalsjökull and Eyjafjallajökull are located on the south coast and are subject to larger temperature variations than, for example, Hofsjökull in the interior, thereby probably also thinning more rapidly than Hofsjökull and northern Vatnajökull. Unfortunately, reliable mass balance data only cover recent years and are primarily observations from Vatnajökull. We therefore chose to use the same constant thinning rate everywhere except in the interior of Vatnajökull.

As discussed in Section 5.2, we know that the Icelandic glaciers grew into the Little Ice Age. Unfortunately, quantitative data on this growth is very scarce. In Section 5.4, we used the Sigmundsson & Einarsson (1992) accumulation rate from 900–1750 AD, which was calculated from the underestimated Vatnajökull ice retreat from 1890 to 1973 of 182 km^3. With the current thinning value of 435 km^3, it is not possible to repeat that calculation in a self-consistent way. Recent modelling of Vatnajökull glacier dynamics (Flowers *et al.* 2005) indicates that the rate of ice accumulation prior to 1800 may be significantly smaller than the volume inferred by Sigmundsson & Einarsson (1992). In addition, a simulation study

on Langjökull by Flowers *et al.* (2008) suggests that the areal extent of Langjökull at the time of settlement was only slightly smaller than the present-day size of the glacier, whereas the maximum was attained about 200 yr ago (their fig. 8). These studies imply that our accumulation rate for ice history (C) is an overestimate and, if so, the difference in results between the (A) and (C) ice histories is even smaller than indicated in Section 5.4. On the other hand, as both the Flowers *et al.* (2005, 2007) studies indicate that the glaciers may have continued to grow into the 19th century, some 50–100 yr longer than our modelled 1750 end-of-growth date, the effect of ice accumulation would be larger, perhaps similar to the effect of our (C) ice history. Since the modelling results using ice history (C) are within the range of uncertainties of the results of ice history (A), it is tempting to conclude (as did Fleming *et al.* 2007, albeit for a slightly different ice history) that an ice accumulation phase prior to 1750 does not affect the results, within the current station distribution and uncertainty levels. In our simulations, we have noted, however, that an ice accumulation phase tends to make the resulting vertical velocities more sensitive to viscosity variations, and therefore has the potential to narrow the range of acceptable viscosities.

Below we discuss the residual vertical uplift rates in the context of sources other than GIA, such as magmatism or earth structure. It is, however, possible that some of the residuals seen in, for example, Fig. 7(b) are caused by errors in the ice model used. It is even possible that some of the residuals could be used to improve estimates of mass balance histories for particular sections of the ice caps.

7.1.3 Structure and rheology of the Earth

In our earth models above, we have used incompressible materials. This is inconsistent with observations of rock properties in seismology and laboratory experiments, which show that Poisson's ratio is approximately 0.25. Including compressibility in our GIA model is non-trivial, as it affects the density of the material and therefore also gravity. Wu (2004) showed how these effects could be incorporated into commercial finite element software through a laborious process which we have not implemented. However, simple so called material compressibility (Klemann *et al.* 2003), i.e. the material's ability to compress under increased stress, can be modelled with our software, (albeit with slight underestimation, see Bängtsson & Lund 2008). It is well known (e.g. Klemann *et al.* 2003) that the buoyancy and gravity effects are of second order but how does material compressibility affect our results? Using compressible (Poisson's ratio 0.25) upper and lower lithospheric layers in our preferred model, the resulting vertical velocities are very similar to the velocities from the incompressible model. The χ^2_ν for the compressible model is 1.90 in comparison to 1.85 for the incompressible model. Using only the vertical rebound velocities we can therefore not distinguish between a compressible and an incompressible Earth. The resulting horizontal velocities, on the contrary, are significantly larger for the compressible model, on average by a factor 1.5. These horizontal velocities will be discussed further below in Section 7.2.

We have modelled the rheological structure beneath Iceland using homogeneous flat elastic and viscoelastic layers overlying a viscoelastic half-space, which is obviously a gross simplification. The three-dimensionality of varying crustal thickness and the mantle plume is likely to affect the resulting GIA velocity field. For example, in a study of the Fennoscandian GIA process Whitehouse *et al.* (2006) found that the inclusion of 3-D structures in the earth model perturbed the 1-D model results enough to exceed the observational uncertainties for continuous GPS recordings. Performing such a 3-D study in our case would result not only in a revised viscosity estimate but also a revised rheological structure for Iceland, which is beyond the scope of this paper. However, we can perhaps gain some insight into the three-dimensionality of the problem by comparing our results of models with different elastic thicknesses. We see in the models in Figs 7(a) and (b) and 9(e) and (f) that the thinner elastic thickness brings out more detail (high-frequency variations) in the vertical velocities than do the thicker elastic layer. Also, the rates in the thinner model are higher close to Vatnajökull than they are in the thicker model. The ISNET data may thus provide a data set which could be used to constrain various lithospheric thickness models of Iceland.

The elastic layer in GIA models is commonly interpreted as the lithosphere, underlain by the viscoelastic asthenosphere. Following this tradition, and using the Allen *et al.* (2002a) estimate of 30 km average crustal thickness, our preferred model would imply a 10-km thick mantle lithosphere beneath Iceland. Our range of possible elastic thicknesses, however, extends down to 80-km depth or more which seems very thick for a region with a ridge-centred mantle plume. We showed that much of this elastic thickness can be substituted with a viscoelastic layer of viscosity of approximately 1×10^{20} Pa s. The small difference in misfit between the lower lithosphere elastic and viscoelastic models suggests nevertheless that the lower lithosphere behaves essentially elastically on the time scale of the current Icelandic glacial rebound. The inferred large elastic thickness could be related to our GPS observations being spread all over Iceland, implying that there are many stations in regions that experience very little rebound (e.g. Fig. 7a). More observations in the vicinity of the glaciers and on nunataks in the ice would undoubtedly put better constraints on the elastic thickness.

Discussions on the thickness of the lithosphere beneath Iceland are few in the literature. Pagli *et al.* (2007a) inferred a 10- to 20-km thick elastic plate but did not test thicker plates. Fleming *et al.* (2007) report a 20- to 30-km thick lithosphere, ranging from 10 to 50 km within 1σ uncertainty. Both these results are within our range of elastic thicknesses. From heat flow data and gravity modelling, Kaban *et al.* (2002) estimate that the 1200°C isotherm is at 30–50 km depth on average below Iceland, which agrees well with our preferred elastic thickness, assuming (as did Kaban *et al.* 2002) that the lithosphere-asthenosphere boundary (LAB) is at approximately 1200°C. At the thicker end of our elastic thickness range are the results of Kumar *et al.* (2005), who infer the LAB at 70-km depth below Iceland from seismic receiver functions and Allen *et al.* (2002b), who place the LAB at 100-km depth using seismic tomography to study the Iceland plume. The seismological LAB may however be quite different from the mechanical LAB, as results from, for example, Scandinavia show (Olsson *et al.* 2007).

The range in our estimated mantle viscosities, $6–15 \times 10^{18}$ Pa s, is similar to recent results from studies of glacial rebound constrained by GPS observations of uplift rates around Vatnajökull, suggesting viscosities in the range of $1–10 \times 10^{18}$ Pa s (e.g. Fleming *et al.* 2007; Pagli *et al.* 2007a). As pointed out above, Fleming *et al.* (2007) used an older estimate of ice thinning rate since 1890, which may explain their lower viscosity estimate. The GPS study by Sjöberg *et al.* (2004) concluded a much lower viscosity of 1×10^{17} Pa s. We can reject such an extremely low value, both because our modelling shows that viscosities below 6×10^{18} Pa s predict uplift rates that are much higher than the vertical rates we observe and because the deglaciation rate used in Sjöberg *et al.* (2004) is more than 50 per cent smaller than the current estimate. The lake levelling measurements from Lake Langisjór reported by Sigmundsson &

Einarsson (1992) indicate a tilt rate of 0.26 ± 0.06 μrad yr^{-1} away from the Vatnajökull ice cap between 1959 and 1991. Our preferred model has a tilt rate of 0.22 μrad yr^{-1}, in agreement with that observation.

Estimates for lower crust and upper mantle viscosities have also been obtained from temporal variation in GPS velocities observed after the Krafla rifting episode (e.g. Hofton & Foulger 1996; Pollitz & Sacks 1996), and the 2000 June earthquakes in South Iceland (e.g. Árnadóttir *et al.* 2005). These studies suggest viscosities ranging from 1–30 × 10^{18} Pa s. Our GIA model estimates therefore fall within this range. LaFemina *et al.* (2005) model rifting cycles in the EVZ to explain GPS station velocities across south Iceland. They find that a half-space viscosity of 10–100 × 10^{18} Pa s, below a thin (<5 km) elastic plate, produces the best fit to their data. The latest major rifting episode in the EVZ was the 1783–1784 Laki eruption (Thordarson & Larsen 2007) and LaFemina *et al.* (2005) conclude that the velocity transient due to this rifting event has dissipated such that the GPS velocities can be fit equally well with elastic half-space dislocation models, which could explain their high viscosity value.

7.2 Residual velocities

An intriguing coherent pattern of residual horizontal motion away from Vatnajökull emerges when we plot the horizontal residual velocities relative to stable Eurasia for stations east and south of the active plate boundary (black arrows in Fig. 11b). As discussed in Section 7.1.3, the GIA models produce horizontal velocities that are significantly higher if we use a compressible earth model, whereas the vertical rates are almost identical. To explore whether the residual horizontal motion we observe in east Iceland could be caused by GIA, we calculate the surface velocities using the preferred GIA model, i.e. a 10-km thick elastic layer over a 30-km thick lower lithosphere with 1 × 10^{20} Pa s, and a half-space with a viscosity of 1 × 10^{19} Pa s, using compressible materials in the upper and lower lithosphere layers. Fig. 13 shows the remaining vertical signal after correcting for the GIA result, including now the stations SKRO, DYNG and 8434. The compressible model predicts vertical velocities that are very similar to Fig. 7(a). The horizontal velocities predicted by the compressible GIA model are shown with red arrows in Fig. 13. The agreement between the GIA model prediction and the observed residual velocities is rather striking, indicating that the GIA causes detectable horizontal motion in the stable parts of eastern and central north Iceland. We did not take horizontal velocities into account in our assessment of GIA models due to the difficulty in separating the relatively small GIA signal from the much larger plate spreading signal and deformation at the active volcanoes. Not being able to use the horizontals is unfortunate since they are valuable for inferences on the rheology of the Earth (Milne *et al.* 2004). The above results indicate that the residual horizontal velocities at selected stations (not affected by local deformation) in eastern Iceland may in fact be used to constrain GIA models.

A fairly persistent pattern of residual vertical velocities is indicated from the GIA modelling for the range of viscosities (1–20 × 10^{18} Pa s) we explored. If the GIA models predict uplift that is faster than the observed velocities, the residual velocities are negative, whereas positive residuals signify GPS station velocities that are higher than the model predictions. The areas with the highest negative residual velocities are located along the plate boundary, i.e. the Reykjanes Peninsula, the WVZ and the southern part of the NVZ (Askja and Kverkfjöll). The GIA models also predict uplift rates that are slightly faster than the observed GPS station velocities in the area around Mýrdalsjökull. Conversely, positive residual velocities appear in the northern part of the NVZ,

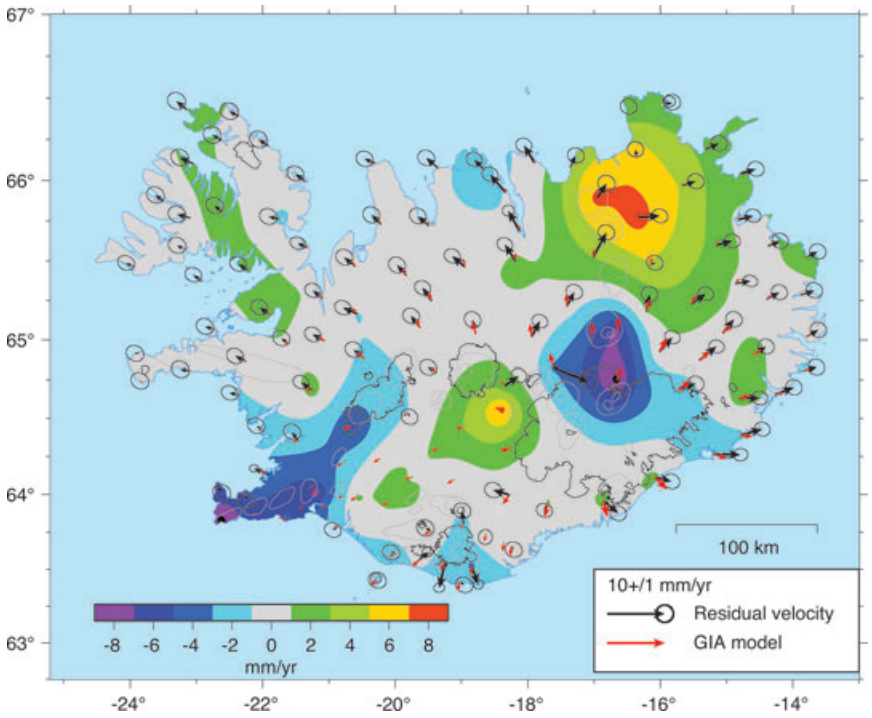

Figure 13. Residual velocities. The black arrows (with 68 per cent confidence ellipses) show the residual horizontal velocities relative to stable North America for stations in the northwest and relative to stable Eurasia for stations in the east and south. The red arrows show the predicted horizontal velocities from the preferred GIA model. The colour scale shows the residual vertical velocities after subtracting the uplift predicted by the preferred GIA model (lower lithosphere and half-space viscosities of 1 × 10^{20} Pa s and 1 × 10^{19} Pa s, respectively) from the vertical ISNET velocities. Positive numbers indicate uplift and negative are subsidence.

extending southeastwards over a wide area in northeast and central Iceland.

7.2.1 Subglacial volcano deformation

It is important to separate uplift caused by glacial rebound from signs of inflation due to magma accumulation at shallow depth beneath subglacial volcanoes. Katla volcano, located beneath Mýrdalsjökull glacier, has shown signs of unrest in the last decade (e.g. Sturkell *et al.* 2008). The pattern of residual velocities in Fig. 13 is a bit perplexing since horizontal motion away from Katla has been interpreted as indication of inflation, whereas the negative residual vertical motion we find, suggests general subsidence. As discussed above, our model of the Mýrdalsjökull and Eyjafjallajökull glaciers is larger than their current extent and some of the GPS sites are thus closer to, and even beneath, the glacier rims in the model. The modelled velocities, both horizontal and vertical, are therefore slightly larger than they should be. A possible reason for the discrepancy of the horizontal and vertical residual motion could be that the ice history that we use for Mýrdalsjökull is incorrect. In order to decrease the uplift predicted by the GIA models, one would, however, need a much slower rate of deglaciation than the 63.4 cm yr^{-1} we use here. If anything, the rate we assume is too slow, at least compared to currently observed thinning rates. Using a faster deglaciation rate would, on the other hand, produce larger horizontal velocities which would fit the horizontal observations better, but further increase the negative vertical residual velocities. Another explanation for the negative vertical residual motion is that the lithosphere in this part of Iceland is thicker and colder than elsewhere. A GIA model with an elastic plate thickness of 80 km and a mantle viscosity of 1×10^{19} Pa s nearly matches the observed uplift rates, but even thicker lithosphere is needed to obtain uplift after correcting the observed vertical rates for the GIA signal. It therefore appears that neither an improved glacial history nor significantly thicker lithosphere suffice to reconcile the horizontal and vertical residuals we observe around Mýrdalsjökull. We therefore suggest that the horizontal motion away from Katla is influenced by deglaciation and that the displacement field is the result of at least two processes, GIA and magmatic movements. Inflation of a shallow level magma chamber leads to a local deformation field that is difficult to detect due to the glacial cover of Katla and the large station spacing in our network. The Katla volcano went through a period of unrest in 1999–2004 expressed in elevated seismicity, increased geothermal activity, a flash-flood and accelerated uplift of nunataks on the caldera rims (Sturkell *et al.* 2008). A combination of GPS-data from a denser network and InSAR data is likely to better constrain contributions of different processes to the total deformation field around Katla volcano.

7.2.2 Vertical deformation outside the ice caps

We observe significant residual uplift over a large area in northeastern Iceland, with a maximum uplift east of Krafla volcano. Magma accumulation at ∼20-km depth was surmised from an InSAR study by de Zeeuw-van Dalfsen *et al.* (2004) spanning 1993–1999. Including this source in our plate boundary model only partly explains the eastward motion of the GPS station 7384 (see Fig. 11b), although our depth resolution is rather poor (10^{-10}_{+8} km). The rate of volume increase ($0.005^{-0.005}_{+0.01}$ $km^3\ yr^{-1}$) is much smaller than the 0.026 $km^3\ yr^{-1}$ obtained by de Zeeuw-van Dalfsen *et al.* (2004). They, however, estimate a spreading rate across the NVZ (34 mm yr^{-1}) that is considerably higher than our estimate of 23 ± 2 mm yr^{-1}. The discrepancy in the parameters we obtain from modelling the ISNET observations and the results from the InSAR study could be due to temporal variation in the spreading rate (modulated by decreasing post-rifting deformation) and/or changes in the rate of deep magma accumulation that we are unable to resolve with the ISNET data. The broad area of significant residual uplift we observe (Fig. 13) appears too extensive to be solely due to magma accumulation at 20-km depth north of Krafla volcano.

We are not able to fully explain the high uplift rate we observe in central Iceland, even when excluding the CGPS station SKRO. As Figs 7 and 9 indicate, the magnitude and extent of the residual uplift, after correcting for the GIA contribution, is very sensitive to the parameters used in the GIA modelling. The broad pattern of residual uplift in central Iceland for the preferred GIA model (Fig. 13) is superimposed by a localized maximum, possibly indicating a shallow source causing the uplift at SKRO. This station is, however, not located in an active volcanic region, and there are no indications of magma accumulation at shallow depth, such as an increase in earthquake activity in the area.

The Askja and Kverkfjöll fissure swarms, and the WVZ through to the tip of the Reykjanes Peninsula, appear to be subsiding at up to 8 mm yr^{-1} (Fig. 13). The last eruption on the RP was in the 13th century, and the last rifting event in the WVZ was in 1789 (Thordarson & Larsen 2007). In general, the WVZ is considered to be a dying rift zone, with most of the spreading accommodated across the EVZ. Lack of magma inflow into the WVZ and the Reykjanes Peninsula may therefore cause the subsidence. The apparent extensive area of subsidence in the Askja and Kverkfjöll fissure swarms is probably an overestimate as a result of the locations of the ISNET stations. InSAR images from 1997 to 1998 show subsidence along the Kverkfjöll and Askja fissure swarms (R. Pedersen, personal communication, 2008). The GPS station 8434, near Kverkfjöll, is subsiding by about 10 mm yr^{-1} after we correct the vertical rate for the GIA signal, which may be partly due to a surge of the outlet glacier Dyngjujökull, as discussed in Section 3.2.

The pattern of horizontal and vertical crustal deformation in Iceland is the result of several different processes, acting at different temporal and spatial scales, and therefore difficult to fully unravel from the data set in this study.

8 CONCLUSIONS

We present a 3-D velocity field for all of Iceland, derived from two GPS campaigns conducted in 1993 and 2004 (ISNET). We supplement the campaign data with data from 16 continuous GPS stations operating in Iceland during the time interval 1999–2004 (Geirsson *et al.* 2006). The vertical velocity field in Iceland shows a high rate of uplift in central Iceland, with a maximum of about 23 mm yr^{-1}, and rates above 10 mm yr^{-1} in a broad area extending from central Iceland towards southeast and northwards. We can explain most of the uplift signal in central and southeast Iceland by GIA due to melting of the largest glaciers in Iceland. The modelling shows that it is necessary to include the smaller glaciers of Langjökull, Hofsjökull, Mýrdalsjökull and Eyjafjallajökull in addition to the large Vatnajökull glacier, in order to fit the observations. Our preferred model has a 10-km thick elastic layer, underlain by a 30-km thick viscoelastic layer with viscosity 1×10^{20} Pa s and a half-space with a viscosity of 1×10^{19} Pa s. We argue that our modelling provides fairly tight constraints on mantle viscosity, in the range $6–15 \times 10^{18}$ Pa s, while the elastic thickness structure above the mantle layer is less well resolved (Fig. 8).

The horizontal velocities show that plate motion across Iceland is primarily accommodated by extension across the northern and

EVZs, with a small amount of spreading in the WVZ and the Reykjanes Peninsula, and transform motion across the TFZ, the SISZ and the Reykjanes Peninsula. A kinematic model of the plate boundary, including several magmatic sources at active volcanoes, matches well the observed horizontal motion. The horizontal velocities we observe for the 1993–2004 time interval across north Iceland are in good agreement with plate motion model predictions. This indicates that the velocity increase observed by early GPS observations at distances greater than 50 km away from the Krafla fissure swarm during 1987–1992, interpreted as post-rifting deformation following the 1975–1984 Krafla rifting episode, has decayed to the steady state spreading rate. A small post-rifting signal is estimated for the time interval 1993–2004, as indicated by the shallow locking depth and the slightly elevated spreading rate of that segment in our plate boundary model and high strain rates. The other segments of the plate boundary model have estimated rates of deep slip or opening that are less than or comparable to the far-field spreading rate in Iceland (about 20 mm yr^{-1}).

Significant residual velocities remain after the vertical velocities are corrected for the GIA signal. We find up to 8 mm yr^{-1} of residual uplift in north Iceland that has been interpreted as signs of deep magma accumulation. The Reykjanes Peninsula and WVZs appear to be subsiding at a rate of about 4–8 mm yr^{-1}, perhaps as a result of lack of magma inflow to this part of the plate boundary. In addition, a spatially coherent pattern of residual horizontal velocities (up to 3 mm yr^{-1}) directed away from Vatnajökull is observed in east Iceland, that is most likely due to GIA. This study exemplifies the complex deformation field generated by many different active processes in Iceland and the need to consider more than one of these when interpreting geodetic data, even in localized studies.

ACKNOWLEDGMENTS

We thank everyone who participated in collecting the vast amount of GPS data used in this study, in particular Gudmundur Valsson, Markus Rennen, Christof Völksen, Erik Sturkell, Theodór Theodórsson, Jón Erlingsson and Halldór Ólafsson. We are grateful to Christof Völksen for providing results from early GPS measurements in north Iceland, to John Haines for sharing his software for the strain calculations and to Rikke Pedersen for sharing her InSAR results. Discussions with Harro Schmeling aided our work on the viscosity structure. Thorough reviews and constructive comments from the Editor (John Beavan) and two reviewers, Christof Völksen and Jeff Freymueller, helped us improve the manuscript. This work was supported in part by grant from the University of Iceland Research Fund. The figures were produced using the GMT public domain software (Wessel & Smith 1998).

REFERENCES

ABAQUS, 2004. ABAQUS manuals, version 6.5, ABAQUS Inc., available at www.abaqus.com [2007 September 20].

Adalgeirsdóttir, G., Björnsson, H., Pálsson, F. & Magnússon, E., 2005. Analyses of a surging outlet glacier of Vatnajökull ice cap, Iceland, *Ann. Glaciol.,* **42,** 23–28, doi:10.3189/172756405781813293.

Ágústsson, K., Stefánsson, R., Linde, A.T., Einarsson, P., Sacks, S.I., Gudmundsson, G.B. & Thorbjarnardóttir, B., 2000. Successful prediction and warning of the 2000 eruption of Hekla based on seismicity and strain changes, *EOS Trans. AGU,* **81**(53), Fall Meet. Suppl., Abstract V11B-30.

Allen, R. *et al.*, 2002a. Plume-driven plumbing and crustal formation in Iceland, *J. geophys. Res.,* **107,** B8, doi:10.1029/2001JB000584.

Allen, R.M. *et al.*, 2002b. Imaging the mantle beneath Iceland using integrated seismological techniques, *J. geophys. Res.,* **107,** 2325, doi:10.1029/2001JB000595.

Altamimi, Z., Collilieux, X., Legrand, J., Garayt, B. & Boucher, C., 2007. ITRF2005: a new release of the International Terrestrial Reference Frame based on time series of station positions and Earth Orientation Parameters, *J. geophys. Res.,* **112,** B09401, doi:10.1029/2007JB004949.

Amelung, F. & Wolf, D., 1994. Viscoelastic perturbations of the Earth: significance of the incremental gravitational force in models of glacial isostacy, *Geophys. J. Int.,* **117,** 864–879.

Antonioli, A., Belardinelli, M., Bizzarri, A. & Vogfjörd, K.S., 2006. Evidence of instantaneous dynamic triggering during the seismic sequence of year 2000 in south Iceland, *J. geophys. Res.,* **111,** B03302, doi:10.1029/2005JB003935.

Árnadóttir, T., Geirsson, H. & Einarsson, P., 2004. Coseismic stress changes and crustal deformation on the Reykjanes Peninsula due to triggered earthquakes on 17 June 2000, *J. geophys. Res.,* **109,** B09307, doi:10.1029/2004JB003130.

Árnadóttir, T., Jónsson, S., Pollitz, F.F., Jiang, W. & Feigl, K.L., 2005. Postseismic deformation following the June 2000 earthquake sequence in the south Iceland seismic zone, *J. geophys. Res.,* **110,** B12308, doi:10.1029/2005JB003701.

Árnadóttir, T., Jiang, W., Feigl, K.L., Geirsson, H. & Sturkell, E., 2006. Kinematic models of plate boundary deformation in southwest Iceland derived from GPS observations, *J. geophys. Res.,* **111,** B07402, doi:10.1029/2005JB003907.

Bängtsson, E. & Lund, B., 2008. A comparison between two solution techniques to solve the equations of glacially induced deformation of an elastic Earth, *Int. J. Numer. Methods Eng.,* **75,** 479–502.

Beavan, J. & Haines, J., 2001. Contemporary horizontal velocity and strain rate fields of the Pacific-Australian plate boundary zone through New Zealand, *J. geophys. Res.,* **106,** 741–770.

Bergthórsson, P., 1969. An estimate of drift ice and temperature in Iceland in 1000 years, *Jökull,* **19,** 94–101.

Beutler, G., Mueller, I. & Neilan, R., 1994. The International GPS service for geodynamics: development and start of official service on January 1, 1994, *Bull. Geod.,* **68,** 39–70.

Björnsson, A., 1985. Dynamics of crustal rifting in Iceland, *J. geophys. Res.,* **90,** 10 151–10 162.

Björnsson, H., 1979. Glaciers in Iceland, *Jökull,* **29,** 74–80.

Björnsson, H. & Pálsson, F., 2008. Icelandic glaciers, *Jökull,* **58,** 365–386.

Björnsson, H., Pálsson, F., Gumundsson, M.T. & Haraldsson, H.H., 1998. Mass balance of western and northern Vatnajökull, Iceland, 1991–1995, *Jökull,* **45,** 35–58.

Björnsson, H., Pálsson, F. & Haraldsson, H.H., 2002. Mass balance of Vatnajökull (1991 – 2001) and Langjökull (1996 – 2001), Iceland, *Jökull,* **51,** 75–78.

Björnsson, H., Pálsson, F., Sigurdsson, O. & Flowers, G.E., 2003. Surges of glaciers in Iceland, *Ann. Glaciol.,* **36,** 82–90.

Bock, Y. *et al.*, 1997. Southern California Permanent GPS Geodetic Array: continuous measurements of regional crustal deformation between the 1992 Landers and 1994 Northridge earthquakes, *J. geophys. Res.,* **102,** 8013–18033.

Bradwell, T., Dugmore, A.J. & Sugden, D.E., 2006. The Little Ice Age glacier maximum in Iceland and the North Atlantic Oscillation: evidence from Lambatungnajökull, southeast Iceland, *Boreas,* **35,** 61–80.

Cervelli, P., Murray, M.H. & Segall, P., 2001. Estimating source parameters from deformation data, with an application to the March 1997 earthquake swarm off the Izu Peninsula, Japan, *J. geophys. Res.,* **106,** 11 217–11 237.

Church, J. & White, N., 2006. A 20th century acceleration in global sea-level rise, *Geophys. Res. Lett.,* **33,** L01602, doi:10.1029/2005GL024826.

Clifton, A.E. & Einarsson, P., 2005. Styles of surface rupture analysis accompanying the June 17 and 21, 2000 earthquakes in the South Iceland Seismic Zone, *Tectonophysics,* **396,** 141–159.

Darbyshire, F.A., White, R.S. & Priestley, K.F., 2000. Structure of the crust and uppermost mantle of Iceland from a combined seismic and gravity study, *Earth planet. Sci. Lett.,* **181,** 409–428.

de Zeeuw-van Dalfsen, E., Pedersen, R., Sigmundsson, F. & Pagli, C., 2004. Satellite radar interferometry 1993–1999 suggests deep accumulation of magma near the crust-mantle boundary at the Krafla volcanic system, Iceland, *Geophys. Res. Lett.,* **31,** L13611, doi:10.1029/2004GL020059.

DeMets, C.G., Gordon, R., Argus, D.F. & Stein, S., 1990. Current plate motions, *Geophys. J. Int.,* **101,** 425–478.

DeMets, C.G., Gordon, R., Argus, D.F. & Stein, S., 1994. Effect of recent revisions to the geomagnetic reversal time scale on estimates of current plate motions, *Geophys. Res. Lett.,* **21,** 2191–2194.

Einarsson, P., 1991. Earthquakes and present-day tectonism in Iceland, *Tectonophysics,* **189,** 261–279.

Einarsson, P. & Sæmundsson, K., 1987. Earthquake epicenters 1982–1985 and volcanic systems in Iceland. A map accompanying festschrift for Th. Sigurgeirsson, in *Í hlutarins edli*, ed. Sigfusson, T., Menningarsjódur, Reykjavík, Iceland.

Einarsson, P., Björnsson, S., Foulger, G., Stefánsson, R. & Skaftadóttir, T., 1981. Seismicity pattern in the South Iceland Seismic Zone, in *Earthquake Prediction – An international review*, Vol. 4, pp. 141–151, eds Simpson, D.W. & Richards, P.G., AGU, Washington D.C.

Feigl, K.L., Gasperi, J., Sigmundsson, F. & Rigo, A., 2000. Crustal deformation near Hengill volcano, Iceland 1993–1998: coupling between magmatic activity and faulting inferred from elastic modeling of satellite radar interferograms, *J. geophys. Res.,* **105,** 25 655–25 670.

Fleming, K., Martinec, Z. & Wolf, D., 2007. Glacial-isostatic adjustment and the viscosity structure underlying the Vatnajökull ice cap, Iceland, *Pure. appl. Geophys.,* **164,** 751–768.

Flowers, G.E., Marshall, S.J., Björnsson, H. & Clarke, G.K., 2005. Sensitivity of Vatnajökull ice cap hydrology and dynamics to climate warming over the next two centuries, *J. geophys. Res.,* **110,** F02011, doi:10.1029/2004JF000200.

Flowers, G.E., Björnsson, H., Geirsdóttir, A., Miller, G.H. & Clarke, G.K., 2007. Glacier fluctuation and inferred climatology of Langjökull ice cap through the Little Ice Age, *Quat. Sci. Rev.,* **26,** 2337–2353.

Flowers, G.E., Björnsson, H., Geirsdóttir, A., Miller, G.H., Black, J.L. & Clarke, G.K., 2008. Holocene climate conditions and glacier variation in central Iceland from physical modelling and empirical evidence, *Quat. Sci. Rev.,* **27,** 797–813.

Foulger, G.R., Jahn, C.H., Seeber, G., Einarsson, P., Julian, B.R. & Heki, K., 1992. Post-rifting stress relaxation at the divergent plate boundary in Northeast Iceland, *Nature,* **358,** 488–490.

Geirsson, H., Árnadóttir, T., Völksen, C., Jiang, W., Sturkell, E., Villemin, T., Einarsson, P. & Sigmundsson, F., 2006. Current plate movements across the Mid-Atlantic ridge determined from 5 years of continuous GPS measurements in Iceland, *J. geophys. Res.,* **111,** B09407, doi:10.1029/2005JB003717.

Geirsson, H. *et al.*, 2007. A new high-rate continuous GPS network in Iceland for crustal deformation research, in *Geophys. Res. Abs.*, EGU2007-A-06993, Vol. 9, European Geosciences Union.

Gíslason, S.R., 2008. Weathering in Iceland, *Jökull,* **58,** 387–408.

Gordon, R.G., 1998. The plate tectonic approximation: plate nonrigidity, diffuse plate boundaries, and global plate reconstruction, *Annu. Rev. Earth Planet. Sci.,* **26,** 615–642.

Grapenthin, R., Sigmundsson, F., Geirsson, H., Árnadóttir, T. & Pinel, V., 2006. Icelandic rhythmics: annual modulation of land elvation and plate spreading by snow load, *Geophys. Res. Lett.,* **33,** L24305, doi:10.1029/2006GL028081.

Gudmundsson, M.T., Sigmundsson, F., Björnsson, H. & Högnadóttir, T., 2004. The 1996 eruption at Gjálp, Vatnajökull ice cap, Iceland: course of events, efficiency of heat transfer, ice deformation and subglacial water pressure, *Bull. Volc.,* **66,** 46–65.

Hanna, E., Jónsson, T. & Box, J.E., 2004. An analysis of Icelandic climate since the nineteenth century, *Int. J. Climatol.,* **24,** 1193–1210.

Hartmann, O., Jacoby, W.R., Wolf, D., Klemann, V. & Sasgen, I., 2007. Interpretation glazial-isostatischer Ausgleichsvorgänge im Südosten Islands unter Berücksichtigung des Island-Plumes, Tech. Rep. STR 07/07, GeoForschungsZentrum Potsdam, in German.

Heki, K., Foulger, G.R., Julian, B.R. & Jahn, C.H., 1993. Plate dynamics near divergent boundaries: geophysical implications of postrifting crustal deformation in NE Iceland, *J. geophys. Res.,* **98**(B8), 14 279–14 298.

Herring, T.A., 2003. GLOBK: global Kalman filter VLBI and GPS analysis program version 4.1, *Tech. Rep., Mass. Inst. Technol.,* Cambridge, MA, USA.

Herring, T.A., Davis, J.L. & Shapiro, I., 1990. Geodesy by radio interferometry: the application of Kalman filtering to very long baseline interferometry data, *J. geophys. Res.,* **95**(B8), 12 561–12 581.

Hjaltadóttir, S., Vogfjörd, K.S. & Slunga, R., 2005. Mapping subsurface faults in southwest Iceland using relatively located microearthquakes, in *Geophys. Res. Abs.*, EGU05-A-06664, Vol. 7, European Geosciences Union.

Hofton, M.A. & Foulger, G.R., 1996. Postrifting anelastic deformation around the spreading plate boundary, north Iceland. 1. Modeling of the 1987–1992 deformation field using a viscoelastic Earth structure, *J. geophys. Res.,* **101**(B11), 25 403–25 422.

Höskuldsson, A., Óskarsson, N., Pedersen, R., Grönvold, K., Vogfjörd, K. & Ólafsdóttir, R., 2007. The millennium eruption of Hekla in February 2000, *Bull. Volc.,* **70,** 169–182.

Hreinsdóttir, S., Einarsson, P. & Sigmundsson, F., 2001. Crustal deformation at the oblique spreading Reykjanes Peninsula, SW Iceland: GPS measurements from 1993 to 1998, *J. geophys. Res.,* **106,** 13 803–13 816.

Ito, G., 2001. Origin of V-shaped Reykjanes Ridges from a pulsing and dehydrating mantle plume, *Nature,* **411,** 681–684.

Jacoby, W., Burger, S., Smilde, P. & Wallner, H., 2001. Temporal gravity variations observed in SE Iceland, *Int. Ridge Crest Res. Arctic Ridges,* **10,** 52–55.

Jahn, C.-H., 1992. Untersuchungen über den Einsatz des Global Positioning Systems (GPS) zum Nachweis rezenter Erdkrustenbewegungen im Spaltengebiet Nordost-Islands, *PhD thesis*, Wissenschaftliche Arbeiten der Fachrichtung Vermessungswesen der Universität Hannover, Nr. 182, Hannover, Germany.

Jakobsdóttir, S.S., Roberts, M.J., Gudmundsson, G.B., Geirsson, H. & Slunga, R., 2008. Earthquake swarms at Upptyppingar, NE Iceland: a sign of magma intrusion? *Stud. Geophys. Geod.,* **52,** 513–528.

Jóhannesson, H., Jakobsson, S. & Sæmundsson, K., 1990. Geolocial map of Iceland, sheet 6, south Iceland, 3rd ed., *Tech. Rep.,* Icelandic Institute of Natural History and Iceland Geodetic Survey, Reykjavík, Iceland.

Kaban, M., Flóvenz, O.G. & Pálmason, G., 2002. Nature of the crust-mantle transition zone and the thermal state of the upper mantle beneath Iceland from gravity modelling, *Geophys. J. Int.,* **149,** 281–299.

Keiding, M., Árnadóttir, T., Sturkell, E., Geirsson, H. & Lund, B., 2008. Strain accumulation along an oblique plate boundary: the Reykjanes Peninsula, southwest Iceland, *Geophys. J. Int.,* **172**(1), 861–872, doi:10.1111/j.1365–246X.2007.03655.x.

King, R.W. & Bock, Y., 2003. Documentation for the GAMIT Analysis Software release 10.1, Tech. Rep., Mass. Inst. Technol., Cambridge, MA, USA.

Klemann, V., Wu, P. & Wolf, D., 2003. Compressible viscoelasticity: stability of solutions for homogeneous plane earth models, *Geophys. J. Int.,* **153,** 569–585.

Kumar, P. *et al.*, 2005. The lithosphere-asthenosphere boundary in the North-West Atlantic region, *Earth Planet. Sci. Lett.,* **236,** 249–257.

LaFemina, P.C., Dixon, T.H., Malservisi, R., Árnadóttir, T., Sturkell, E., Sigmundsson, F. & Einarsson, P., 2005. Geodetic GPS measurements in south Iceland: strain accumulation and partitioning in a propagating ridge system, *J. geophys. Res.,* **110,** B11405, doi:10.1029/2005JB003675.

Lund, B., 2005. Effects of deglaciation on the crustal stress field and implications for endglacial faulting: a parametric study of simple Earth and ice models, Tech. Rep. TR-05-04, Swedish Nuclear Fuel and Waste Managment Co. (SKB), Stockholm, Sweden.

Marshall, S.J., Björnsson, H., Flowers, G.E. & Clarke, G.K., 2005. Simulation of Vatnajökull ice cap dynamics, *J. geophys. Res.,* **110,** F03009, doi:10.1029/2004JF000262.

McClusky, S. et al., 2000. Global Positioning System constraints on plate kinematics and dynamics in the eastern Mediterranean and Caucasus, *J. geophys. Res.,* **105**(B3), 5695–5720.

McKinzey, K.M., Orwin, J.F. & Bradwell, T., 2005. A revised chronology of key Vatnajökull (Iceland) outlet glaciers during the Little Ice Age, *Ann. Glaciol.,* **42,** 171–179.

Menke, W., West, M., Brandsdóttir, B. & Sparks, D., 1998. Compressional and shear velocity structure of the lithosphere in northern Iceland, *Bull. seism. Soc. Am.,* **88,** 1561–1571.

Milne, G.A., Mitrovica, J.X., Scherneck, H.-G., Davis, J.L., Johansson, J.M., Koivula, H. & Vermeer, M., 2004. Continuous GPS measurements of postglacial adjustment in Fennoscandia: 2. modeling results, *J. geophys. Res.,* **109,** B02412, doi:10.1029/2003JB002619.

Moberg, A., Sonechkin, D., Holmgren, K., Datsenko, N. & Karlén, W., 2005. Highly variable Northern Hemisphere temperatures reconstructed from low- and high-resolution proxy data, *Nature,* **443,** 613–617.

Olsson, S., Roberts, R. & Bödvarsson, R., 2007. Analysis of waves converted from S to P in the upper mantle beneath the Baltic Shield, *Earth planet. Sci. Lett.,* **257,** 37–46.

Pagli, C., Sigmundsson, F., Árnadóttir, T., Einarsson, P. & Sturkell, E., 2006. Deformation of the Askja volcanic system: constraints on the deformation source from combined inversion of satellite radar interferograms and GPS measurements, *J. Volc. Geotherm. Res.,* **152,** 97–108.

Pagli, C., Sigmundsson, F., Lund, B., Sturkell, E., Geirsson, H., Einarsson, P., Árnadóttir, T. & Hreinsdóttir, S., 2007a. Glacio-isostatic deformation around the Vatnajökull ice cap, Iceland, induced by recent climate warming: GPS observations and finite element modeling, *J. geophys. Res.,* **112,** B08405, doi:10.1029/2006JB004421.

Pagli, C., Sigmundsson, F., Pedersen, R., Einarsson, P., Árnadóttir, T. & Feigl, K.L., 2007b. Crustal deformation associated with the 1996 Gjálp subglacial eruption, Iceland: InSAR studies in affected areas adjacent to the Vatnajökull ice cap, *Earth planet. Sci. Lett.,* **259,** 24–33.

Pedersen, R. & Sigmundsson, F., 2004. InSAR based sill model links spatially offset areas of deformation and seismicity for the 1994 unrest episode at Eyjafjallajökull volcano, Iceland, *Geophys. Res. Lett.,* **31,** L14610, doi:10.1029/2004GL020368.

Pedersen, R. & Sigmundsson, F., 2006. Temporal development of the 1999 intrusive episode in the Eyjafjallajökull volcano, Iceland, derived from InSAR images, *Bull. Volc.,* **68,** doi:10.1007/s00445–005–0020–y.

Pedersen, R., Jónsson, S., Árnadóttir, T., Sigmundsson, F. & Feigl, K.L., 2003. Fault slip distribution of two $M_w = 6.5$ earthquakes in South Iceland estimated from joint inversion of InSAR and GPS measurements, *Earth planet. Sci. Lett.,* **213,** 487–502.

Pinel, V., Sigmundsson, F., Sturkell, E., Geirsson, H., Einarsson, P., Gudmundsson, M.T. & Högnadóttir, T., 2007. Discriminating volcano deformation due to magma movements and variable surface loads: application to Katla subglacial volcano, Iceland, *Geophys. J. Int.,* **169,** 325–338.

Pollitz, F.F. & Sacks, I.S., 1996. Viscosity structure beneath northeast Iceland, *J. geophys. Res.,* **101,** 17 771–17 793.

Rögnvaldsson, S.T., Gudmundsson, Á. & Slunga, R., 1998. Seismotectonic analysis of the Tjörnes Fracture Zone, an active transform fault in north Iceland, *J. geophys. Res.,* **103,** 30 117–30 129.

Sæmundsson, K., 1992. Geology of the Thingvallavatn area, *Oikos,* **64,** 40–67.

Schmeling, H. & Marquart, G., 2008. Crustal accretion and dynamic feedback on mantle melting of a ridge centred plume: the Iceland case, *Tectonophysics,* **447,** 31–52.

Sella, G.F., Dixon, T.H. & Mao, A., 2002. REVEL: a model for recent plate velocities from space geodesy, *J. geophys. Res.,* **107,** ETG 11–1–31, doi:10.1029/2000JB000033.

Sigmundsson, F. & Einarsson, P., 1992. Glacio-isostaic crustal movements caused by historical volume change of the Vatnajökull ice cap, Iceland, *Geophys. Res. Lett.,* **19,** 2123–2126.

Sigmundsson, F., Einarsson, P., Bilham, R. & Sturkell, E., 1995. Rift-transform kinematics in south Iceland: deformation from Global Positioning System measurements, 1986 and 1992, *J. geophys. Res.,* **100,** 6235–6248.

Sigmundsson, F., Einarsson, P., Rögnvaldsson, S.T., Foulger, G.R., Hodgkinsson, K.M. & Thorbergsson, G., 1997. The 1994–1995 seismicity and deformation at the Hengill triple junction, Iceland: triggering of earthquakes by minor magma injection in a zone of horizontal shear stress, *J. geophys. Res.,* **102**(B7), 15 151–15 161.

Sjöberg, L.-E., Pan, M., Erlingsson, S., Asenjo, E. & Arnason, K., 2004. Land uplift near Vatnajökull, Iceland, as observed by GPS in 1992, 1996 and 1999, *Geophys. J. Int.,* **159,** 943–948.

Soosalu, H., White, R., Key, A., Knox, C., Einarsson, P. & Jakobsdóttir, S.S., 2008. Lower-crustal earthquakes reflect magma movements beneath the north Iceland rift near Askja, in *Geophys. Res. Abs.*, EGU2008-A-07323, Vol. 10, European Geosciences Union.

Stefánsson, R., Gudmundsson, G. & Halldórsson, P., 2003. The South Iceland earthquakes 2000 – a challenge for earthquake prediction research, Tech. Rep. VI-R03017, Icelandic Meteorological Office, Reykjavík, Iceland.

Sturkell, E., Einarsson, P., Sigmundsson, F., Hreinsdóttir, S. & Geirsson, H., 2003. Deformation of Grímsvötn volcano, Iceland: 1998 eruption and subsequent inflation, *Geophys. Res. Lett.,* **30**(4), 1182, doi:10.1029/2002GL016460.

Sturkell, E., Sigmundsson, F. & Slunga, R., 2006. 1983–2003 decaying rate of deflation at Askja caldera: pressure decrease in an extensive magma plumbing system at a spreading plate boundary, *Bull. Volc.,* **68,** 727–735.

Sturkell, E. *et al.*, 2008. Seismic and geodetic insights into magma accumulation at Katla subglacial volcano, Iceland: 1999 to 2005, *J. geophys. Res.,* **113,** B03212, doi:10.1029/2006JB004851.

Thoma, M. & Wolf, D., 2001. Inverting land uplift near Vatnajökull, Iceland, in terms of lithosphere thickness and viscosity stratification, in *Gravity, Geoid and Geodynamics 2000*, pp. 97–102, ed. Sideris, M., Springer-Verlag, Berlin.

Thórarinsson, S., 1943. Oscillations of the Iceland glaciers in the last 250 years, *Geografiska Annaler,* **25,** 1–54.

Thordarson, T. & Larsen, G., 2007. Volcanism in Iceland in historical time: volcano types, eruption styles and eruptive history, *J. Geodyn.,* **43,** 118–152.

Tryggvason, A., Rögnvaldsson, S.T. & Flóvenz, O.G., 2002. Three-dimensional imaging of the P- and S-wave velocity structure and earthquake locations beneath Southwest Iceland, *Geophys. J. Int.,* **151,** 848–866.

Tryggvason, E., 1994. Surface deformation at the Krafla volcano, north Iceland, 1982–1992, *Bull. Volc.,* **56,** 98–107.

Valsson, G.T., Sigurdsson, T., Völksen, C. & Rennen, M., 2007. ISNET2004. Results from a resurvey of the Icelandic geodetic reference network (in Icelandic with an English summary), Tech. Rep., National Land Survey of Iceland, Akranes, Iceland.

Vogfjörd, K.S., Hjaltadóttir, S. & Slunga, R., 2005. Volcano-tectonic interaction in the Hengill region, Iceland during 1993–1998, in *Geophys. Res. Abs.*, EGU05-J-09947, Vol. 7, European Geosciences Union.

Völksen, C., 2000. Die Nutzung von GPS für die Deformationsanalyse in regionalen Netzen am Beispiel Islands, *PhD thesis*, Wissenschaftliche Arbeiten der Fachrichtung Vermessungswesen der Universität Hannover, Nr. 237, Hannover, Germany.

Wessel, P. & Smith, W., 1998. New, improved version of generic mapping tools released, *EOS, Trans. Am. geophys. Un.,* **79,** 579.

Whitehouse, P., Latychev, K., Milne, G.A., Mitrovica, J.X. & Kendall, R., 2006. Impact of 3-D Earth structure on Fennoscandian glacial isostatic adjustment: implications for space-geodetic estimates of present day crustal deformations, *Geophys. Res. Lett.,* **33,** L13502, doi:10.1029/2006GL026568.

Wolfe, C., Bjarnason, I.T., VanDecar, J.C. & Solomon, S.C., 1997. Seismic structure of the Iceland mantle plume, *Nature,* **385,** 245–247.

Wu, P., 1992. Deformation of an incompressible viscoelastic flat earth with power-law creep: a finite element approach, *Geophys. J. Int.,* **108,** 35–51.

Wu, P., 2004. Using commercial finite element packages for the study of earth deformations, sea levels and the state of stress, *Geophys. J. Int.,* **158,** 401–408, doi:10.1111/j.1365–246X.2004.02338.x.

SUPPORTING INFORMATION

Additional Supporting Information may be found in the online version of this article:

Appendix S1. Supplementary Tables S1–S3 referenced in the text.

Please note: Wiley-Blackwell are not responsible for the content or functionality of any supporting materials supplied by the authors. Any queries (other than missing material) should be directed to the corresponding author for the article.